

Mitigating Traffic Oscillations in Mixed Traffic Flow with Scalable Deep Koopman Predictive Control

Hao Lyu^{a,b,c}, Yanyong Guo^{a,b,c,*}, Pan Liu^{a,b,c}, Nan Zheng^d, Ting Wang^e and Quansheng Yue^{a,b,c}

^aSchool of Transportation, Southeast University, Nanjing, China, 211189

^bJiangsu Key Laboratory of Urban ITS, Nanjing, China, 210096

^cJiangsu Collaborative Innovation Center of Modern Urban Traffic Technologies, Nanjing, China, 210096

^dDepartment of Civil Engineering, Institute of Transport Studies, Monash University, Melbourne, Australia, VIC 3800

^eCollege of Transportation Engineering, Tongji University, Shanghai, PR China, 201804

ARTICLE INFO

Keywords:

Mixed traffic flow
Connected automated vehicles
Data-driven predictive control
Koopman operator theory
Mitigating traffic oscillations

ABSTRACT

The use of connected automated vehicle (CAV) is advocated to mitigate traffic oscillations in mixed traffic flow consisting of CAVs and human driven vehicles (HDVs). This study proposes an adaptive deep Koopman predictive control framework (AdapKoopPC) for regulating mixed traffic flow. Firstly, a Koopman theory-based adaptive trajectory prediction deep network (AdapKoopnet) is designed for modeling HDVs car-following behavior. AdapKoopnet enables the representation of HDVs behavior by a linear model in a high-dimensional space. Secondly, the model predictive control is employed to smooth the mixed traffic flow, where the combination of the linear dynamic model of CAVs and linear prediction blocks from AdapKoopnet is embedded as the predictive model into the AdapKoopPC. Finally, the predictive performance of the prosed AdapKoopnet is verified using the HighD naturalistic driving dataset. Furthermore, the control performance of AdapKoopPC is validated by the numerical simulations. Results demonstrate that the AdapKoopnet provides more accuracy HDVs predicted trajectories than the baseline nonlinear models. Moreover, the proposed AdapKoopPC exhibits more effective control performance with less computation cost compared with baselines in mitigating traffic oscillations, especially at the low CAVs penetration rates. The code of proposed AdapKoopPC is open source¹.

1. Introduction

With the acceleration of urbanization and the increase in the number of motor vehicles, traffic congestion and traffic accidents have become increasingly prominent Bansal, Graham et al. (2023); Yan and Wang (2022). Against this background, autonomous driving technology has emerged and is expected to become an innovative solution to alleviate traffic congestion Wang, Wang, Jiang, Zhu, Yan and Shang (2024b); Ma and He (2024). The most common application is Cooperative Adaptive Cruise Control (CACC), which relies on V2V state sharing to enable vehicles within a vehicle platoon to run at coordinated speeds to maintain a small headway Dey, Yan, Wang, Shen, Chowdhury, Yu, Qiu and Soundararaj (2015); Wang, Zhou, Liu and Peeta (2024a); Shen and Du (2024). This technique can enhance traffic capacity and improve safety between vehicles, which has attracted a lot of interest from academia and industry. The excellent performance of Connected Automated Vehicle (CAV) in a purely intelligent network environment has been widely recognized Durrani and Lee (2024); Alanazi (2023). In essence, CAV is a mobile scanner that provides historical and real-time trajectory data of individual vehicles Ahmadian, Bahrami, Nourinejad and Yin (2025). As well, it is also a dynamic actuator for adaptive control Du, Makridis, Tampère, Kouvelas and ShangGuan (2023); Guo and Ban (2023). In this intelligent network ideal scenario, vehicles communicate seamlessly and autonomous driving systems operate together accurately and efficiently, thus building a highly intelligent transportation ecosystem Wang, Bian, Shladover, Wu, Li and Barth (2019). However, the industrialization of autonomous driving technology is a complex process, and the realization of large-scale application of mobile internet and autonomous driving technology is a long process Talebian and Mishra (2018). A more realistic traffic environment is that CAVs and Human-Driven Vehicles (HDVs) share the road. This mixed traffic flow prompts scholars to think deeply and study the performance

¹<https://github.com/SpaceTrafficSafetyTeam/AdapKoopPC>

 lyu_hao@seu.edu.cn (H. Lyu); guoyanyong@seu.edu.cn (Y. Guo); liupan@seu.edu.cn (P. Liu); nan.zheng@monash.edu (N. Zheng); 2110763@tongji.edu.cn (T. Wang); yue_qs@seu.edu.cn (Q. Yue)
ORCID(s): 0000-0002-1664-8050 (H. Lyu)

1 of CAVs in complex traffic environments Wang, Lu and Peeta (2022); Cui, Cao, Yu and Yao (2021). Considering
2 the research topics of this paper, we mainly focus on the following two key points, including the modeling of HDVs
3 behavior and the controlling of CAVs.

4 **How to model the HDVs driving behavior in dynamic traffic flow, and to predict the HDVs trajectory with**
5 **high accuracy?** A key goal is to simulate the dynamic driving behaviors of HDVs in mixed traffic flow. These be-
6 haviors will be essentially different due to differences in driving environments, drivers, etc. HDV adjusts its own
7 acceleration based on the headway to the leader vehicle, velocity difference, and among others. In term of the physics-
8 driven methods, well-known car-following models were widely employed, such as optimal velocity model Bando,
9 Hasebe, Nakanishi and Nakayama (1998), full velocity difference model Jiang, Hu, Zhang, Gao, Jia and Wu (2015),
10 intelligent driver model Treiber, Hennecke and Helbing (2000), to describe and model the HDVs behaviors. How-
11 ever, it is known that these time-invariant car-following models always archives high-biased results with large error.
12 With the rapid development of artificial intelligence, big data and computing power, the deep learning methods, in-
13 cluding recurrent neural networks (RNN), long short-term memory model (LSTM), deep deterministic policy gradient
14 (DDPG), etc., are being gained more and more interests in modeling the driving behaviors of HDVs. Although deep
15 learning is superior in capturing and modeling driving behavior in complex traffic environments, due to the character-
16 istic of nonlinearity, its shortcomings of slow solution speed and inability to meet real-time optimization control are
17 self-evident.

18 **How to control CAVs more effectively in mixed traffic flows for mitigating traffic oscillations?** As well known,
19 the jam-absorption driving strategy in the Newell's car-following theory framework was proposed to mitigate the prop-
20 agation of upstream disturbances, and the corresponding vehicles need to be selected based on the expected absorption
21 speed and real-time traffic conditions to implement the strategy Nishi, Tomoeda, Shimura and Nishinari (2013); Li,
22 Yanagisawa and Nishinari (2024). As mentioned before, CAV is a dynamic executor, and its role is no longer limited
23 to "follower", but has been further expanded to "leader", which is the basic idea and connotation of the Leading Cruise
24 Control (LCC) framework Wang, Zheng, Chen, Xu and Li (2021). In addition, the controllability, observability and
25 head-to-tail stability of the LCC framework were also analyzed and verified, confirming its positive role in improving
26 traffic performance Zheng, Wang and Li (2020); Wang, Zheng, Xu, Wang and Li (2020). Along this direction, the
27 Data-Enabled Predictive Leading Cruise Control (Deep-LCC) was proposed Wang, Zheng, Li and Xu (2023b); Wang,
28 Lian, Jiang, Xu, Li and Jones (2023a), as an alternative to parametric car-following model, to achieve safe and optimal
29 control of CAVs in mixed platoons. The Deep-LCC has inspired this paper, however, it still exhibits certain limita-
30 tions. To be specific, in order to use CAVs to positively guide HDVs, it is necessary to first understand the driving
31 behavior changes of HDV after being affected by CAVs. In Deep-LCC, all HDVs follow OVM/IDM and add random
32 high-frequency noise to construct the trajectory database. It is obviously unrealistic and limited to combine these tra-
33 jectories to match the corresponding HDV expected driving trajectories for different scenarios. this is obviously not
34 realistic and has limitations.

35 Overall, the dilemmas faced by CAV control for traffic optimization in mixed traffic flow lies in accurately modeling
36 and predicting the driving behavior of HDVs in complex scenarios, as well as meeting the requirements of effective and
37 feasible real-time solution and optimization control in reality. Motivated by the above two requirements, the Koopman
38 operator offers a new solution for identifying and analyzing nonlinear systems. The Koopman operator emerges as a
39 highly suitable approach, which facilitates the handling of intricate nonlinear dynamics through linear transformations.
40 This method allows for an efficient modeling of the HDVs behavior without introducing excessive complexity, and its
41 linear properties are well suited for subsequent real-time optimization of mixed traffic flow. Therefore, this paper
42 develops a multi-scenario adaptive deep Koopman predictive control framework for mixed traffic flow. The main
43 contributions of this paper are as follows:

- 44 • The deep Koopman network-based trajectory prediction model (AdaptKoopnet) is developed to simulate and
45 predict the complex car-following behavior of HDVs under different driving scenarios. AdaptKoopnet directly
46 learns and extracts potential scenarios and driving characteristics from naturalistic driving trajectory data, with-
47 out relying on pre-labels;
- 48 • The AdapKoopnet-based predicted control framework, AdapKoopPC, is proposed for real-time control of CAVs
49 in mixed traffic flow. AdapKoopPC can adaptively adopt multiple AdapKoopNets to form a mixed traffic system
50 based on the vehicle composition of the local mixed flow, and then implement the control strategy
- 51 • The experiments are designed and conducted to validate the effectiveness and superiority performance of Adap-

1 Koopnet and AdapKoopPC framework proposed in this paper, covering small-scale traffic systems (10 vehicles)
2 and large-scale traffic systems (50 vehicles) with lower CAVs penetration rates. The results demonstrate the
3 ability of AdapKoopPC to reduce traffic flow oscillations and improve traffic flow stability.

4 The framework of this paper is as follows. Section 2 mainly reviews the relevant literatures and summarizes the
5 research gap. Section 3 states the AdapKoopnet. Section 4 proposes the AdapKoopPC framework. Section 5 and
6 Section 6 conducts the experiments for HDVs longitudinal trajectory prediction and mixed traffic flow optimization
7 control. At last, the conclusion and prospects are given in Section 7 .

8 **2. Related work**

9 **2.1. Driving scenario and characteristics recognition**

10 Recognizing and extracting potential driving scenarios is beneficial for achieving vehicle trajectory prediction
11 with strong generalization ability and accuracy. Montanari, German and Djanatliev (2020) extracted driving scenarios
12 directly from real driving data and clustered repeated patterns into potential scenario groups without any pre-definition
13 or rules. Jarl, Aronsson, Rahrovani and Chehreghani (2022) develops a general active learning framework to annotate
14 driving trajectory time series data and explore unknown driving scenario trajectories. Beyond scenario recognition,
15 more research focuses on capturing driving characteristics. Zou, Zhu, Xie, Zhang and Zhang (2022) considered the
16 interaction between driving behavior variables and fully extracted the potential driving patterns, thereby achieving the
17 acquisition of driving behavior semantics and the comparison of the similarity of different driving styles. Li, Chen,
18 Cao, Qu, Cheng and Li (2021) utilized unsupervised algorithms to automatically extract descriptive driving patterns,
19 and the clustered patterns promote a comprehensive understanding of driver behavior characteristics. In addition,
20 efficiently and stably identifying the driving style is also a work with practical value. For example, based on the multi-
21 dimensional characteristics, a specific driving style is generated for each vehicle, and three different driving styles
22 are further identified using an unsupervised clustering algorithmXing, Lv and Cao (2019). Gao, Cai, Qu, Hu and
23 Chen (2020) employed a set of experiments to collect driving data among different drivers, and a supervised machine
24 learning-based driving style classifier was designed to recognize the driving style. Zhang, Chen, Wang, Zheng and Wu
25 (2022) defined the intermediate variable of neural process as the driving style vector and linked to an interpretable and
26 continuous aggressiveness index. However, identifying and clustering scenarios from natural driving datasets using
27 neural networks without relying on pre-definition or pre-labeling remains to be solved. Secondly, further extracting
28 personalized driving features based on recognized scenarios and using them for driving behavior prediction is also
29 worth exploring.

30 **2.2. Car following behavior modeling and trajectory prediction**

31 The trajectory prediction methods of car-following behavior are mainly divided into physics-based methods, data-
32 driven methods, and hybrid-driven methods. The physics-based method uses microscopic traffic flow models for tra-
33 jectory prediction. For example, Gindelé, Brechtel and Dillmann (2010) explicitly considered the interactions between
34 vehicles and proposed a dynamic Bayesian networks-based filter to estimate the behavior of traffic participants and pre-
35 dict their future trajectories. Zhou, Qu and Jin (2016) developed a cooperative intelligent driver model that dynamically
36 determines its acceleration based on parameters such as velocity difference and headway. With the advancement of
37 big data and deep learning technology, data-driven methods for trajectories prediction have been emerging. Lin, Li, Bi
38 and Qin (2021) built spatiotemporal attention long short-term memory (STA-LSTM) for vehicle trajectory prediction,
39 ensuring accuracy while improving interpretability. Zhang, Sun, Qi and Sun (2019) uses long short-term memory
40 neural network to automatically extract features that affect car-following and lane-changing behaviors, and then adopt
41 time series data and memory effects to predict driving behavior. Physics-based models or purely data-driven models ei-
42 ther produce unsatisfactory predictive performance or lack the interpretability and physical implications of the model.
43 Pioneeringly, Mo, Shi and Di (2021) first proposed a physics informed deep learning framework for car-following
44 modeling, taking full advantage of data-driven and physics-based models to surpass existing models. Further, relying
45 on the self-attention mechanism to achieve deeper mining of trajectory features, Geng, Li, Xia and Chen (2023) pro-
46 posed a Physics-Informed Transformer-Intelligent Driver Model to predict longitudinal vehicle trajectories. However,
47 there is still a contradiction between the complex deep learning model that describes the nonlinear state evolution of
48 vehicle driving behavior and the requirement that CAV control relies on real-time solutions.

1 2.3. CAV control for optimized mixed traffic flow

2 Various control approaches have been explored to optimize mixed traffic flow performance such as safety, efficiency
3 and energy consumption. Feng, Song, Li, Zhang and Li (2021) presented a highly efficient platoons control frame-
4 work based on tube MPC to address heavy computational and communication burden, which dynamically mitigates
5 prediction uncertainty through feedback control. Shi, Zhou, Wu, Wang, Lin and Ran (2021) divided mixed traffic into
6 sub-platoons and implemented a cooperative control strategy for CAVs under the assumption of completely random
7 disturbances triggered by HDVs. Recently, a control strategy called “The Follower Stopper controller” (FS) was pro-
8 posed, and real vehicle experiments demonstrated its ability to improve traffic flow stability Stern, Cui, Delle Monache,
9 Bhadani, Bunting, Churchill, Hamilton, Pohlmann, Wu, Piccoli et al. (2018). To address the limitation of executing FS
10 policies individually for all CAVs, Wang, Jiang, Wu and Yao (2024c) considered CAV driving behavior and established
11 a cellular automaton model of mixed traffic flow based on the follower stopper controller strategy for CAV control,
12 which positively affected the efficiency, oscillation, and fuel consumption of mixed traffic flow. From the perspective
13 of collective function optimization, Li, Wang and Zheng (2022) studied the impact of different formations of CAVs
14 on traffic performance, focusing on the formation of cooperation between CAVs using centralized optimal controllers.
15 Besides, a traffic-smoothing controller was directly learned from trajectories based on a reinforcement learning policy
16 gradient algorithm Lichtlé, Vinitsky, Nice, Seibold, Work and Bayen (2022). Yue, Shi, Zhou and Li (2024) integrated
17 an advanced linear controller and a DPPO-based DRL controller to construct a hybrid controller, achieving stable and
18 efficient longitudinal driving of CAVs within mixed flow. Zhao and Yu (2024) developed the robust-safety-critical
19 traffic controller in mixed traffic flow. This controller ensures collision-free safety even in the face of actuator and
20 sensor delays, as well as disturbances from the leading HV. As traffic systems expand, a consequent problem is the
21 dramatic increase in online computing burden, and the data-driven distributed control emerged as the times require.
22 Surprisingly, Zhan, Ma and Zhang (2022) conducted data-driven mixed vehicle platoons dynamics modeling based on
23 Koopman, which is a groundbreaking work that has attracted our high attention and interest. Wang et al. (2023b,a)
24 proposed distributed data-driven predictive control that directly utilizes measurable traffic data to design collision-free
25 optimal CAV control inputs for collaboratively smoothing mixed traffic flows. However, it is difficult to demonstrate
26 its generalization ability in other mixed traffic flow scenarios by modeling the entire traffic flow and obtaining the
27 Koopman operator based on a dataset generated by simple physical models, which drives our idea. We expect to use
28 Koopman theory to learn vehicle features from real-world trajectories and construct a scene adaptive and scalable
29 control framework.

30 2.4. The applications of Koopman operator theory in traffic flow

31 Koopman operator theory is a mathematical framework that involves representing nonlinear systems in a higher-
32 dimensional linear space, making it possible to study the evolution of complex systems Koopman (1931) . Avila
33 and Mezić (2020) used Koopman operator to propose a model-free, data-driven approach that cleverly analyzed and
34 predicted the evolution of highly complex nonlinear traffic flow. Ling, Zheng, Ratliff and Coogan (2020) applied
35 Koopman operator theory and the dynamical mode decomposition (DMD) for signalized traffic flow networks control,
36 which allows for early identification of unstable queue growth. In order to realize the real-time control of the ramp
37 metering on the freeway efficiently, Gu, Zhou and Wu (2023) proposed a model predictive controller with the trained
38 deep Koopman model. The above methods relied on parameter estimation of physical models or modeling of nonlinear
39 dynamics using neural networks. Xiao, Zhang, Xu, Liu and Liu (2022) introduced a novel data-driven vehicle model-
40 ing and control approach, employing an interpretable Koopman operator base deep neural networks in which extended
41 dynamic mode decomposition was utilized to learn a finite-dimensional approximation of the Koopman operator. Re-
42 cent studies have further advanced the application of Koopman operator theory in traffic flow. Tian, Shi, Zhou and Li
43 (2024) developed an AI-driven Koopman approach to model nonlinear platoon dynamics during traffic oscillations,
44 combining deep learning with physical interpretability to enhance accuracy and stability analysis. Li, Wang, Yang,
45 Xu, Wang and Li (2025) proposed a robust nonlinear data-driven predictive control framework for mixed vehicle pla-
46 toons, leveraging the Koopman operator to map nonlinear dynamics to a linear space and incorporating reachability
47 analysis to handle noise and disturbances effectively. However, a common limitation of these studies is their reliance
48 on learning the Koopman operator directly from vehicle platoon trajectory data with a fixed number of vehicles, which
49 may limit scalability to diverse or larger traffic systems.

1 **3. AdapKoopnet: Adaptive deep Koopman network for car following behavior modeling**
2 **and prediction of HDVs**

3 In this section, a data-driven adaptive deep Koopman linear model is proposed to address the challenges associated
4 with real-time cognition and prediction of the state of HDVs.

5 **3.1. Key terms definition**

6 Considering that terms such as scenarios have different understandings in existing research. Here we define and
7 explain several key terms that apply specifically to this paper:

8 *Scenario* is the mixed traffic flow environment in which the vehicle is located, such as free flow, synchronous flow,
9 congestion flow, etc., and the direct explicit status includes traffic flow velocity, density, etc.

10 *Scenario characteristics* refers to the collective driving behavior exhibited by drivers in corresponding scenes,
11 which is a potential common feature. For example, in high-velocity and high-density driving scenario, drivers generally
12 pay more attention to the behavior of surrounding vehicles, are greatly influenced by them, and adjust their own driving
13 behavior more frequently than usual.

14 *Driving characteristics* is the specific manifestations of an individual driver's long-term driving habits in differ-
15 ent driving scenarios. For example, aggressive drivers may be more conservative in high-velocity and high-density
16 scenarios compared to free flow scenarios. However, this tendency is uncertain. Some drivers exhibit driving char-
17 acteristics similar to the average of vehicle group characteristics in certain scenarios, while others are only slightly
18 affected. Therefore, the predicted scenario classification is the comprehensive value of driver tendency and scenario
19 characteristics themselves.

20 **3.2. Problem description**

21 Assuming that in high-density mixed traffic flow, HDVs not engaging in lane-changing behavior are primarily influ-
22 enced by their preceding vehicles. Their driving behavior is primarily shaped by the current velocity of the preceding
23 vehicle, their own current velocity, and the headway. For the purpose of research, time is discretized into infinitesi-
24 mally small segments, and the aforementioned process can be described by the following equationsSaifuzzaman and
25 Zheng (2014):

$$(v_i(t+1), h_i(t+1)) = f(v_i(t), h_i(t), v_{i-1}(t)) \quad (1)$$

26 where $v_i(t)$, $h_i(t)$, $v_{i-1}(t)$ respectively represent the velocity, headway of vehicle i , and the velocity of the preceding
27 vehicle $i - 1$ at time t ; $f()$ denotes the state transition function.

28 In real-world scenarios, different drivers commonly exhibit markedly diverse behaviors when faced with identi-
29 cal situations. This variability is intricately associated with individual driving habits, short-term fluctuations in the
30 surrounding environment, and specific driving intentions.

31 These short-term trajectories serve as external manifestations of driver characteristics, encapsulating abundant driv-
32 ing semantic information. Consequently, they are employed for the identification and differentiation of heterogeneity
33 among drivers. Therefore, the problem is defined as follows:

$$\begin{aligned} dc_i(t) &= f_{dc}(x_i(t-P), x_i(t-P+1), x_i(t)) \\ (v_i(t+1), h_i(t+1)) &= f_{sp}(v_i(t), h_i(t), dc_i(t), v_{i-1}(t)) \end{aligned} \quad (2)$$

34 where $x_i(\cdot) = [v_i(\cdot), h_i(\cdot), \Delta v_i(\cdot), a_i(\cdot), l_i]$, $\Delta v_i(\cdot)$, $a_i(\cdot)$, l_i respectively represent the velocity difference, accel-
35 eration, and vehicle length of vehicle i ; P , $f_{dc}(\cdot)$, $dc_i(\cdot)$ respectively represent the length of historical trajectories, the
36 mapping relationship between trajectories and driving characteristics, and the driving characteristics extracted from
37 information containing P trajectory samples.

38 As illustrated in Eq. (2), the objective in this section revolves finding a mapping. The inputs contain the historical
39 trajectory context, the current explicit state of the vehicle i , the velocity of the preceding vehicle $i - 1$, and the outputs
40 contain the prediction velocity and headway of the vehicle i in next time step. However, the mapping is typically
41 nonlinear, leading to significant computational delays in online optimization for mixed traffic flow. The Koopman
42 operator theory provides an promising approach to tackle this challenge.

1 **3.3. Koopman operator theory for state prediction of HDVs**

2 **3.3.1. Koopman operator theory**

3 The Koopman operator theory initially provides an alternative linear dynamic description for the evolution of
 4 uncontrollable systems Koopman (1931). With slight modifications, the Koopman operator can be applied to controlled
 5 systems Proctor, Brunton and Kutz (2018). Therefore, the evolution of system modeled by Eq. (2) can be expressed
 6 by a linear Koopman operator in an infinite-dimensional space. Let $z_i(\cdot) = [v_i(\cdot), h_i(\cdot), d c_i(\cdot)]^T \in \mathbb{Z}$ represents the
 7 state of vehicle i , $\mathbf{v}_{i-1}(t) = v_0^\infty$ denotes all the velocities in the velocity space V , the Koopman operator on System
 8 corresponding to Eq.(2) with the extended state $[z_i(t), \mathbf{v}_{i-1}(t)]$ is defined as follows:

$$\mathcal{K}\phi(z_i(t), \mathbf{v}_{i-1}(t)) = \phi(z_i(t+1), \mathbf{v}_{i-1}(t+1)) = \phi(f_{sp}(z_i(t), \mathbf{v}_{i-1}(t)) + \vartheta\mathbf{v}_{i-1}(t)) \quad (3)$$

9 where \mathcal{K} is the Koopman operator in the infinite-dimensional space; $\vartheta\mathbf{v}_{i-1}(t) = \mathbf{v}_{i-1}(t+1)$ with ϑ being a left shift
 10 operator. It is noteworthy that, unlike $f_{dc}(\cdot)$ directly acting on the state $z_i(\cdot)$, the Koopman operator \mathcal{K} operates on
 11 the state space functions $\phi(\cdot) \in \mathbb{Z} \times V$ with $\phi : \mathbb{Z} \times V \rightarrow \mathbb{C}$. Exploiting the linearity of \mathcal{K} , it can be subjected to
 12 eigenvalue decomposition, expressed as follows:

$$\mathcal{K}\phi_m(z_i(t), \mathbf{v}_{i-1}(t)) = \lambda_m \phi_m(z_i(t), \mathbf{v}_{i-1}(t)) \quad (4)$$

13 where λ_m , $\phi_m(\cdot)$ represent the eigenvalues of \mathcal{K} and their corresponding eigenfunctions, respectively. The future states
 14 of the system can be acquired either by directly evolving $z_i(\cdot)$ or by evolving the complete observable state through
 15 the Koopman operator:

$$f_{sp}(z_i(t), \mathbf{v}_{i-1}(t)) = \sum_{m=1}^{\infty} \lambda_m v_m \phi_m(z_i(t), \mathbf{v}_{i-1}(t)) \quad (5)$$

16 where v_m is the Koopman mode corresponding to the eigenvalue λ_m . The relationship between the original space and
 17 the observable infinite-dimensional space is depicted in Fig. 1.

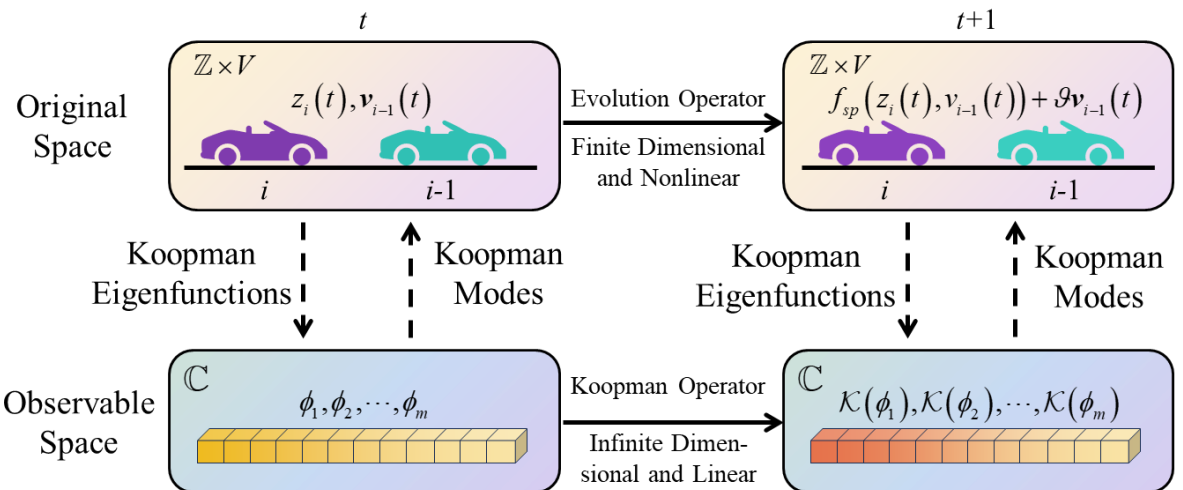


Figure 1: The relationship between the original space and the observable space

18 Based on Eqs. (3)-(5), the endeavor to derive a global linearized dynamic description equivalent to system modeled
 19 by Eq.(2) involves the search for Koopman eigenvalues along with their corresponding eigenfunctions and Koopman
 20 modes. Nevertheless, the Koopman operator typically encompasses an infinite number of eigenvalues. Consequently,
 21 in most instances, a global linear approximation of the system can only be achieved by identifying essential eigenvalues
 22 and their associated eigenfunctions and Koopman modes.

1 **3.3.2. Extended dynamic mode decomposition**

2 The extended dynamic mode decomposition (EDMD) is a data-driven approach of finding the finite-dimensional
 3 approximation K of the Koopman operator Williams, Kevrekidis and Rowley (2015). EDMD employs various basis
 4 functions, such as Radial Basis Functions (RBF) with different kernel centers and widths, to represent observable
 5 functions. It utilizes least squares regression to calculate K . For forced dynamics model in Eq. (2), a special way for
 6 selecting basis functions is defined in Eq. (5) to obtain :

$$\phi(z_i(t), \mathbf{v}_{i-1}(t)) = [\varphi(z_i(t))^T, \mathbf{v}_{i-1}(t)^T]^T \quad (6)$$

7 where $\varphi(\cdot) = [\varphi_1(\cdot)^T \ \varphi_2(\cdot)^T \ \dots \ \varphi_L(\cdot)^T]^T$ represents a set of observable lift functions is general nonlinear. Let $s_i(k) =$
 8 $\varphi(z_i(k))$, combining Eqs. (3)-(6), Eq. (7) is obtained:

$$\phi(z_i(k+1)) = \mathcal{K}\phi(z_i(k), v_{n-1}(k)) = \mathcal{K}[s_n(k)^T v_{n-1}(k)^T]^T + r \quad (7)$$

9 where r is residual term that describes the gap between the L -dimensional approximation of the observable space and
 10 the actual lifted space of the Koopman operator, used to determine the optimal \mathcal{K} . However, selecting the lifting
 11 functions for the complex dynamics of System (2) poses a challenge, and advanced deep learning techniques are
 12 employed to learn \mathcal{K} .

13 **3.4. Model architecture**

14 A deep learning model, based on attention mechanisms and feedforward networks, is constructed to accomplish
 15 the following tasks: 1) Extracting latent driving characteristics from historical trajectory context, which are utilized to
 16 aid in understanding and predicting the behavior of HDVs; 2) Learning Koopman lifting functions, Koopman operator
 17 approximation, and Koopman modes, the latter two of which are linear, for online optimization in CAVs .

18 The model architecture is depicted in Fig.2. For trajectory context inputs, the model incorporates a driving char-
 19 acteristic semantic extraction block (highlighted by the deep green dashed box in Fig.2). To handle the current vehicle
 20 state input, a multi-layer perceptron-based encoder-lifting function approximation is employed. The fusion gate mech-
 21 anism integrates the encoding of driving characteristics with the explicit state encoding of the lifting space, yielding
 22 the state of the observable high-dimensional Koopman space approximation. By incorporating the future velocity of
 23 the preceding vehicle into the network, the model adaptively learns the Koopman operator approximation and achieves
 24 multi-step state predictions in the high-dimensional space. This module is denoted as the Koopman evolution block,
 25 highlighted by the pink dashed box in Fig.2). Additionally, a linear decoder, serving as an approximation for Koopman
 26 modes, is utilized to transform observations from the high-dimensional space to obtain predicted states in the original
 27 space.

28 **3.4.1. Driving characteristic semantic extraction block**

29 As shown in Fig. 2, this block takes trajectory context as input, containing details as specified in the Eq. (2),
 30 and outputs a vector representing the current latent driving characteristics of the driver. The block comprises an
 31 input embedding and temporal encoding (ITE) module, a multi-head dynamic temporal interaction (DTI) module, a
 32 multi-head driving scenario recognition (DSR) module, and a driving characteristics semantic transformation (DCSE)
 33 module, each of which is detailed below.

34 **Input Embedding and Temporal Encoding (ITE) Module** The input embedding layer serves to convert the trajec-
 35 tory context into a high-dimensional dense representation, allowing the model to comprehensively learn the trajectory
 36 features and analyze correlation between trajectory samples. The embedding is achieved through a fully connected
 37 layer with a ReLU activation function. Given that the embedding operation is conducted for each trajectory sample, a
 38 relative time encoding method is introduced to enable subsequent modules to recognize the temporal information of
 39 trajectory context Vaswani, Shazeer, Parmar, Uszkoreit, Jones, Gomez, Kaiser and Polosukhin (2017). The expression
 40 is as follows:

$$TE_{(t,2i)} = \sin\left(\frac{t}{10000^{(2i/d_{model})}}\right) \quad (8)$$

$$TE_{(t,2i+1)} = \cos\left(\frac{t}{10000^{(2i/d_{model})}}\right)$$

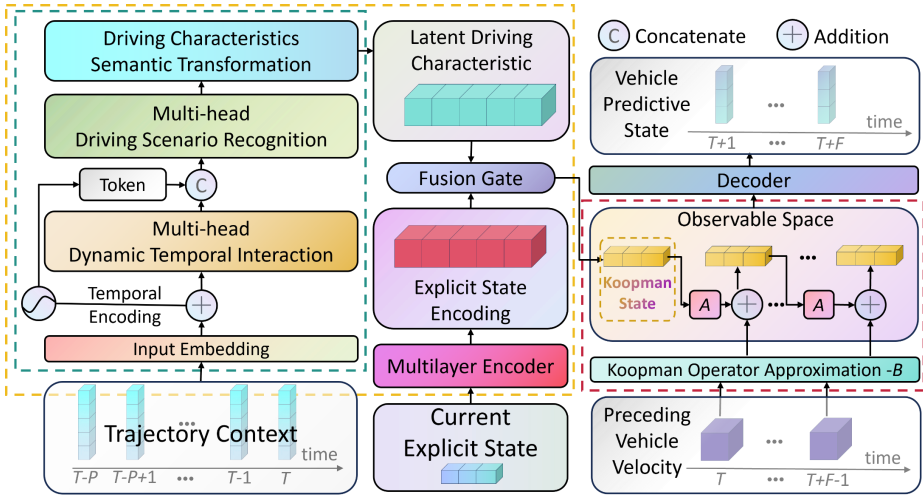


Figure 2: The model architecture of AdapKoopnet

1 where i, t represent the encoding feature dimension index and time step, respectively; d_{model} represents the dimension-
2 ability of the encoding of each module in the AdaptKoopnet, without special declaration. Subsequently, the trajectory
3 context input embedding and temporal encoding are added together to form the output of this module. The expression
4 is as follows:

$$H_{ITE} = \text{ReLU}(W_{IE} \cdot (x(T-P), x(T-P+1), x(T)) + b_{IE}) + TE \quad (9)$$

5 where W_{IE}, b_{IE} , represent the weights and biases of the input embedding layer.

6 **Multi-Head Dynamic Temporal Interaction (DTI) Module** The vehicle state undergoes continuous changes, and
7 there exists a strong interaction and correlation between trajectory samples. This module leverages multi-head atten-
8 tion and feedforward layers to capture and understand the temporal interactions and dependencies within the vehicle
9 trajectory context. Firstly, the multi-head attention mechanism projects the output of ITE into multiple subspaces. In
10 each subspace, it independently learns interaction features within the trajectory context and facilitates feature exchange.
11 By focusing on different subspaces, the model can better capture information from different dimensions within the tra-
12 jectory context, enhancing its ability to model complex relationships between trajectory sequences. This approach not
13 only accelerates the speed of training and inference but also contributes to a more comprehensive understanding of the
14 intricate dynamics among trajectory samples.

15 The dimension of each subspace is also a hyperparameter. In AdapKoopnet, a uniform subspace dimension is
16 adopted and denoted as d_{att} . The calculation formula for \bar{H}_{DTI} in the figure is as follows:

$$\begin{aligned} Q_{DTI}^h &= W_{DTI-q}^h H_{ITE}, \quad Q_{DTI}^h = W_{DTI-k}^h H_{ITE}, \quad Q_{DTI}^h = W_{DTI-v}^h H_{ITE} \\ \bar{H}_{DTI}^h &= \text{softmax}\left(\frac{Q_{DTI}^h K_{DTI}^h}{\sqrt{d_{att}}}\right) V_{DTI}^h \\ \bar{H}_{DTI} &= LN\left(W_{DTI-att}\left(\left\|_{g=1}^H \bar{H}_{DTI}^h\right\| + H_{ITE}\right)\right) \end{aligned} \quad (10)$$

17 where $W_{DTI-q}^h, W_{DTI-k}^h, W_{DTI-v}^h, W_{DTI-att}$ represents learnable weights; $\|\cdot\|$ denotes the concatenate operation.
18 $LN(\cdot)$ stands for Layer Normalization, a technique that normalizes the trajectory encoding along the feature dimension

1 to mitigate the impact of internal covariate shift Ba, Kiros and Hinton (2016). Unlike Batch Normalization (BN), Layer
2 Normalization is more flexible as it is not influenced by the size of the data batch.

3 After achieving feature exchange within the trajectory context through the attention layer, the feedforward layer Fine
4 (2006) is employed for the nonlinear transformation of trajectory encoding. This aims to capture the nonlinear rela-
5 tionships within the trajectory context, facilitating the model in learning higher-level abstract representations. The
6 feedforward layer consists of two linear transformations and an activation function. Initially, \bar{H}_{DTI} undergoes a fully
7 connected layer, followed by the application of the ReLU activation function, and finally passes through another fully
8 connected layer. After \bar{H}_{DTI} goes through the feedforward layer, the output of the DTI module is obtained, calculated
9 using the following formula:

$$H_{DTI} = LN \left(W_{DTI-FFN}^2 (\text{ReLU} (W_{DTI-FFN}^1 (\bar{H}_{DTI}))) + \bar{H}_{DTI} \right) \quad (11)$$

10 where $W_{DTI-FFN}^1$ and $W_{DTI-FFN}^2$ represent the weights of the feedforward layer in the DIT module.

11 **Multi-Head Driving Scenario Recognition (DSR) Module** Following the extracting and initial abstracting of
12 temporal interaction characteristics within the trajectory context through the DTI module, the cognitive understanding
13 of driving scenario and the extraction of driving characteristic semantics become crucial steps. This is because, in
14 different driving scenarios, even for the same driver, driving characteristics may vary. For example, in scenarios with
15 large headway, drivers may not require to remain highly vigilant about their preceding vehicles, and their driving
16 behavior tends to be smoother. Conversely, in high-density and high-velocity scenarios, drivers may concentrate more
17 on monitoring changes in the state of preceding vehicle and respond more actively. The DSR module learns scenario
18 information hidden within the trajectory context by adapting to relevant feature variations from a vast set of driving
19 trajectory contexts. It dynamically recognizes and classifies the driving scenario in which the vehicle is situated.

20 Fig. 3 (a) illustrates the structure of the DSR module. Initially, Eq. (8) is utilized to generate a special encoding
21 token. Subsequently, this token is concatenated with the output of the DTI module H_{DTI} , functioning as the original
22 query. The role of this token is to extract features conducive to the cognitive understanding of driving scenarios
23 by attending to the trajectory context encoding. These features undergo further abstraction through the nonlinear
24 transformation of the feedforward layer. The module was associated and matched these abstracted features with the
25 learned scenario information features of the model, achieving cognitive recognition and prediction of implicit driving
26 scenarios within the trajectory context. Similar to the DTI module, this module conduct deep exchange and further
27 abstraction of interaction features within the trajectory context.

28 The computational process of the DSR module is fundamentally similar to the DTI module. Its output in the
29 feedforward layer is as follows:

$$H_{DSR-DS}, H_{DSR-TC} = \bar{W}_{DSR} (SE, H_{DTI}) \quad (12)$$

30 where SE , \bar{W}_{DSR} , H_{DSR-TC} and H_{DSR-DS} represent the special encoding token, the weights of DSR module,
31 the trajectory context encoding in Figure 4, and the special encoding token that completes the extraction of driving
32 scenario features, respectively. H_{DSR-DS} undergoes a linear layer to aggregate driving scenario features, resulting in
33 a vector with the same dimension as the predefined number of scenes. After applying the softmax activation function,
34 the driving scenario prediction vector depicted in Fig. 3 (a) is obtained. Each dimension of this vector represents
35 the predicted probability of the trajectory context belonging to the corresponding scene. The formula is expressed as
36 follows:

$$H_{DS} = \text{softmax} (W_{DSR-DS} \cdot (H_{DSR-DS})) \quad (13)$$

37 **Remark 1:** In this study, real labels for driving scenario are not available. Therefore, the driving scenario recogni-
38 tion process involves a spontaneous classification process by the neural network based on a large amount of trajectory
39 context. At the inception of the network design, the task of the DSR module is to cluster recurring trajectory pat-
40 terns and interpret the generated clusters as potential scenarios. From a macro perspective, this lays the foundation
41 for extracting semantic characteristics of driving characteristics. In Section 5, explicit features corresponding to each
42 scenario will be visualized, although this may not necessarily be the sole basis for the classification of network.

43 **Driving Characteristics Semantic Transformation (DCSE) Module** As mentioned in the DSR module, driving
44 characteristics vary across different driving scenarios. The current module aims to perform driving characteristic

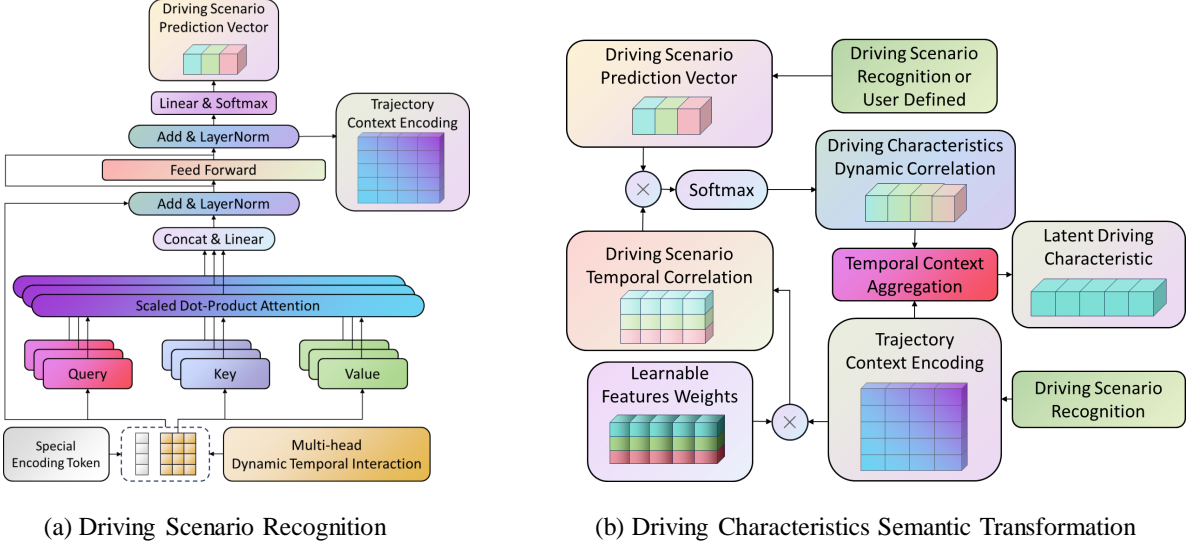


Figure 3: The architecture of DSR module and DCSE module

1 semantic extraction guided by the predicted results of driving scenario recognition. The structural diagram of module
2 is presented in Fig. 3 (b).

3 The process begins by defining learnable feature weights corresponding to each scenario. These weights dynam-
4 ically learn the importance of each feature in the trajectory context encoding under predefined scenarios, using an
5 extensive training data. The features are then aggregated based on the learned importance, obtaining the relevance of
6 each trajectory sample to driving characteristic extraction in a specific driving scenario. Then, the relevance for each
7 scenario is aggregated based on the probabilities predicted by the DSR module or according to user-defined scenarios.
8 After applying the softmax activation function, the correlation between the trajectory context encoding and driving
9 features is obtained. Based on this correlation, the trajectory context is aggregated, ultimately revealing the driving
10 features hidden within the trajectory context. The computational formula for this module is as follows:

$$dc(T) = \text{softmax}(H_{DSR-TC} d_{sf_c} H_{DS})^T H_{DSR-TC} \quad (14)$$

11 where d_{sf_c} , dc_T respectively represent the learnable feature weights corresponding to each scenario, and the latent
12 driving characteristic at time T .

13 3.4.2. Explicit state encoder and fusion gate mechanism

14 The explicit state encoder is tasked with encoding the explicit state of the vehicle from the original space to an
15 observable high-dimensional space, facilitating the action of the Koopman lifting function on the current vehicle state.
16 This encoder initially embeds the vehicle state into a high-dimensional representation through a linear layer with a
17 ReLU activation function. Subsequently, a Multi-Layer Perceptron (MLP) with tanh activation function is utilized to
18 perform multiple linear transformations on the embedded representation, completing the task of encoding the explicit
19 state of the vehicle. Next, the explicit state encoding and the latent driving characteristics of the vehicle need to be
20 fused to form the Koopman state approximation for the current time step. The Gated Linear Unit (GLU) is introduced
21 to accomplish this fusion task. It employs a gate mechanism to adaptively filter redundant features and retain essential
22 features Dauphin, Fan, Auli and Grangier (2017). The computational formula for the above process is as follows:

$$\begin{aligned} es(T) &= W_{ESE} \cdot es(T) \\ s(T) &= W_{FG} \cdot (dc(T), es(T)) \end{aligned} \quad (15)$$

23 where $es(T) = (v(T), h(T))^T$; W_{ESE} , W_{FG} represents the weights of explicit state encoder and fusion gate mech-
24 nism, respectively. $es(T)$, $s(T)$ represent the explicit state encoding and Koopman state approximation of the vehicle

1 at time step T .

2 3.4.3. Koopman evolution block and decoder

3 In the Koopman evolution block, the multi-step evolution in the observable high-dimensional linear system is
4 achieved based on the Koopman operator approximation K learned through two linear layers without bias. Specifically,
5 K comprises the system matrix A and the control matrix B . A describes the process of system state transition
6 without control inputs, while the velocity of preceding vehicle in the prediction horizon is treated as the system control
7 input. This input is applied to the system through the control matrix B to complete the system evolution. The formal
8 expression of this process is as follows:

$$9 \begin{aligned} s^P(T+F) &= As^P(T+F-1) + Bv_{-1}(T+F-1) \\ &= A^F s(T) + \sum_{f=1}^F A^{f-1} B v_{-1}(T+F-f) \\ &\stackrel{\Delta}{=} \tilde{A}^F(s(T), v_{-1}(T : T+F-1)) \end{aligned} \quad (16)$$

9 where $s^P(\cdot)$, $v_{-1}(\cdot)$ represent the predicted state in high-dimensional space and the velocity of the preceding vehicle,
10 respectively.

11 Subsequently, the decoder, characterized as a bias-free linear layer, serves to approximate the Koopman modes
12 and reconstruct the predicted state from the observable high-dimensional space to the original space. To minimize
13 online computation delay for CAVs, the decoder is specifically designed as a linear layer without bias (In Section 5, the
14 predictive performance difference between the current decoder and using an MLP as the decoder will be demonstrated).
15 The reconstructed state variables in the original space align with the state variables input to the explicit state encoder
16 in AdapKoopnet. The reconstruction process is expressed as follows:

$$17 es^P(T+f) = W_{DEC} \cdot s^P(T+f) \quad (17)$$

17 where $es^P(T+f) = (v^P(T), h^P(T))^T$ represents the predicted state of the original space; W_{DEC} represents the
18 learnable weights in the decoder.

19 **Remark 2:** In a typical trajectory prediction task, incorporating future velocities of the preceding vehicle as inputs
20 may be impractical. However, the primary objective of AdapKoopnet is to predict the response driving behavior of
21 HDVs to the preceding vehicle. This facilitates subsequent inferences about the required velocity of the CAVs. This
22 makes this setup appear much more reasonable.

23 3.5. Loss function

24 Loss of AdapKoopnet is composed of reconstruction error, prediction error, and linear evolution error Lusch, Kutz
25 and Brunton (2018). Specifically, the reconstruction error represents the difference between the reconstructed state
26 obtained by embedding the current explicit state of the vehicle into a high-dimensional space and reconstructing it
27 through the decoder, and the original state. To achieve accurate reconstruction of the original state, the reconstruction
28 error for the entire prediction horizon is included as part of the loss function, expressed as follows:

$$29 L_C = \frac{1}{F+1} \sum_{f=0}^F \left\| \varphi^d(\varphi^e(es(T+f), x(T-P+f : T+f))) - es(T+f) \right\| \quad (18)$$

29 where $\varphi^d(\cdot)$, $\varphi^e(\cdot)$ represent the transformations performed by the encoding block (highlighted by the yellow dashed
30 box in Figure 2) and the decoder in AdapKoopnet; $\|\cdot\|$ represents mean squared error. The prediction error represents
31 the difference between the predicted state and the ground truth, and it is defined as:

$$32 L_P = \frac{1}{F} \sum_{f=1}^F \|es^P(T+f) - es(T+f)\| \quad (19)$$

32 The linear evolution error represents the difference between the Koopman state approximation at time T after F steps
33 of linear evolution and the Koopman state approximation at time $T+F$. It is defined as:

$$L_E = \|s^P(T + F) - s(T + F)\| \quad (20)$$

¹ The loss function of AdapKoopnet is expressed as:

$$L = \alpha_C L_C + \alpha_P L_P + \alpha_E L_E \quad (21)$$

² where $\alpha_C, \alpha_P, \alpha_E$ are the weights corresponding to the three parts of the loss, and they are hyperparameters. To avoid
³ manually selecting hyperparameters, Dynamic Weight Average (DWA) are introduced Liu, Johns and Davison (2019).
⁴ These weights are adjusted based on the losses from the previous epoch in the dynamic loss function.

⁵ 4. AdapKoopPC: Predictive control framework of CAVs for real-time optimizing mixed ⁶ traffic flow based on Adakoopnet

⁷ 4.1. Problem description and system state representation

⁸ Consider a local traffic system within a high-density mixed traffic flow, as illustrated in Fig. 4 consisting of N
⁹ HDVs and G CAVs driving in the same lane. The leading vehicle is a HDV numbered as 0. For convenience, CAVs
¹⁰ are sequentially numbered as 1, 2, ..., G . The HDVs located between CAV g and $g + 1$ are sequentially numbered as
¹¹ $g1, g2, \dots, gn_g$. The equivalence relationships exist: $\sum_{g=1}^G gn_g = N$. Assuming that all HDV states in this system can be
¹² collected through the onboard sensors of CAVs or a V2X (Vehicle-to-Everything) system. The control problem of this
¹³ system is defined as achieving the following objectives through the rolling optimization of control inputs for CAVs:
¹⁴ (1) Minimizing the velocity difference between any two adjacent vehicles in the system, while maintaining reasonable
¹⁵ headway to alleviate traffic oscillations transmitted by the leading vehicle. (2) Ensuring that the velocities of vehicles
¹⁶ in the system are close to that of the leading vehicle, aiming to mitigate oscillations while maintaining traffic efficiency.

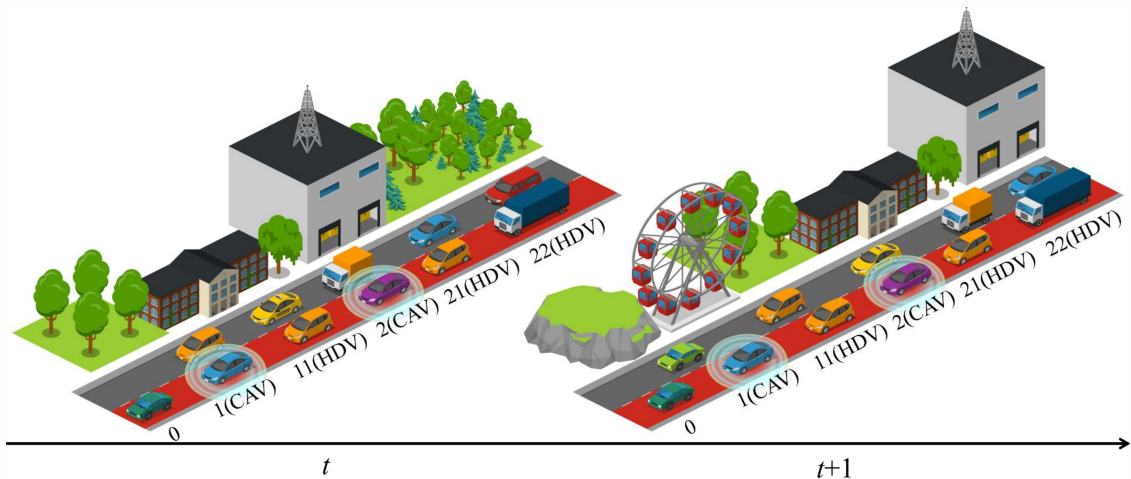


Figure 4: The local mixed traffic system

¹⁷ Based on the above two objectives and for the convenience of constraint formulation, the system state is defined as
¹⁸ follows:

$$ES(t) = (p_1(t), v_1(t), a_1(t), h_{11}(t), v_{11}(t), \Delta v_{11}(t), \dots, h_{Gn_G}(t), v_{Gn_G}(t), \Delta v_{Gn_G}(t)) \quad (22)$$

¹⁹ where $ES(t)$ encompasses the headways, velocities of all vehicles in the system, as well as the velocity differences of
²⁰ HDVs and accelerations of CAVs; $p_1(t)$ is the position of the first CAV in the system. The control input of the system

1 is defined as the jerk of CAVs, i.e., the rate of change of acceleration, denoted as:

$$U(t) = (u_1(t), u_2(t), \dots, u_G(t)) \quad (23)$$

2 **Remark 3:** In large-scale high-density mixed traffic flow scenarios, the lane-changing frequency is low, areas
 3 without lane changes occur can be divided into multiple systems as described above. The system lacks a strict organi-
 4 zational structure, requiring cooperation among a few neighboring CAVs to establish. Unlike most existing research,
 5 the achievement of control objectives of the system does not depend on the so-called equilibrium velocity and equilib-
 6 rium headway. Minimizing the velocity difference between adjacent vehicles is more readily accepted by HDV drivers,
 7 aligns with their own driving objectives in most cases. For scenarios with low penetration rates of V2X systems, sim-
 8 ulation experiments relying solely on the onboard sensors of CAVs are conducted and tested in Section 6.

9 4.2. State predictive model of mixed traffic system

10 To enable the rapid convergence of the system to the desired state while satisfying the constraints on system states
 11 and control inputs, a predictive control framework is adopted. The framework assumes a set of feasible control input
 12 sequences within a specified region known as the control horizon N_C . Based on the predictive model, a series of
 13 predictive states within the predictive horizon N_P is obtained. By minimizing the error between the reference state
 14 and the predictive state, the optimal control input that satisfies constraints is determined. The current step control input
 15 is then applied to the CAVs, and this iterative process ensures that the control input at each step for the CAVs is at
 16 least a suboptimal solution. It is evident that in this framework, the accuracy of the system state predictive model is
 17 crucial. Firstly, the CAVs in the system are controllable, and their predictive state is obtained through the following
 18 vehicle kinematics equations:

$$\begin{aligned} p_q(t+1) &= p_q(t) + v_q(t) \cdot \Delta t \\ v_q(t+1) &= v_q(t) + a_q(t) \cdot \Delta t \\ a_q(t+1) &= a_q(t) + u_q(t) \cdot \Delta t \end{aligned} = \begin{bmatrix} 1 & \Delta t & 0 \\ 0 & 1 & \Delta t \\ 0 & 0 & 1 \end{bmatrix} \cdot \begin{bmatrix} p_q(t) \\ v_q(t) \\ a_q(t) \end{bmatrix} + \begin{bmatrix} 0 \\ 0 \\ \Delta t \end{bmatrix} \cdot u_q(t) \quad (24)$$

19 where $\begin{bmatrix} 1 & \Delta t & 0 \\ 0 & 1 & \Delta t \\ 0 & 0 & 1 \end{bmatrix} \triangleq A_{CAV}$, $\begin{bmatrix} 0 \\ 0 \\ \Delta t \end{bmatrix} \triangleq B_{CAV}$ represent the system matrix and state matrix of CAVs, respectively. In
 20 this system, there is always at least one CAV in front of any HDV. Therefore, AdapKoopnet can be cascaded to predict
 21 the states of all vehicles in the system under specific control inputs of CAVs. This forms the basis for resolving traffic
 22 flow stop-and-go waves in the framework. The predictive process for all HDVs is illustrated in Fig. 5. Prior to the
 23 predictive process, it is necessary to obtain the high-dimensional representation of the current state of the vehicles
 24 using the encoding block of AdapKoopnet.

25 However, the predictive process seems to be cumbersome, particularly when system involves numerous vehicles.
 26 Therefore, the state predictive model needs to be integrated before initiating prediction to perform parallel prediction
 27 of all vehicle states within the system. For any HDV in system, the following relationship exists:

$$\begin{cases} s_{gn_g}(t+1) = A \cdot s_{gn_g}(t) + B \cdot v_{gn_g-1}(t) \\ es_{gn_g}(t) = C \cdot s_{gn_g}(t) \end{cases} \quad (25)$$

28 where C represents the observation matrix, which is the linear decoder in AdaptKoopnet. For the HDVs, where the
 29 preceding vehicle is also an HDV, the following equations are further obtained:

$$s_{gn_g}(t+1) = A \cdot s_{gn_g}(t) + B \cdot C_v \cdot s_{gn_g}(t) \quad (26)$$

30 where C_v represents the row in the observation matrix used for observing velocity. Combining Eqs. (22)-(26), the
 31 predictive model for the system is obtained:

$$\begin{cases} S(t+1) = A_S \cdot S(t) + B_S \cdot U(t) \\ ES(t) = C_S \cdot S(t) \end{cases} \quad (27)$$

1 where

$$S(t) = \begin{bmatrix} p_1(t), v_1(t).a_1(t), s_{11}(t), \dots, h_g(t), v_g(t).\Delta v_g(t), \dots, s_{gn_g}(t), \dots, s_{Gn_G}(t) \end{bmatrix}^T$$

$$A_S = \begin{bmatrix} A_{CAV} & & & & \\ B & A & & & \\ BC_v & & A & & \\ & \ddots & \ddots & \ddots & \\ & & A_{CAV} & & \\ & & & \ddots & \ddots \end{bmatrix}, B_S = \begin{bmatrix} B_{CAV} & & & \\ & \ddots & & \\ & & B_{CAV} & \\ & & & \ddots \end{bmatrix}, C_S = \begin{bmatrix} I_3 & & & \\ & C & & \\ & & \ddots & \\ & & & I_3 \end{bmatrix}$$

(28)

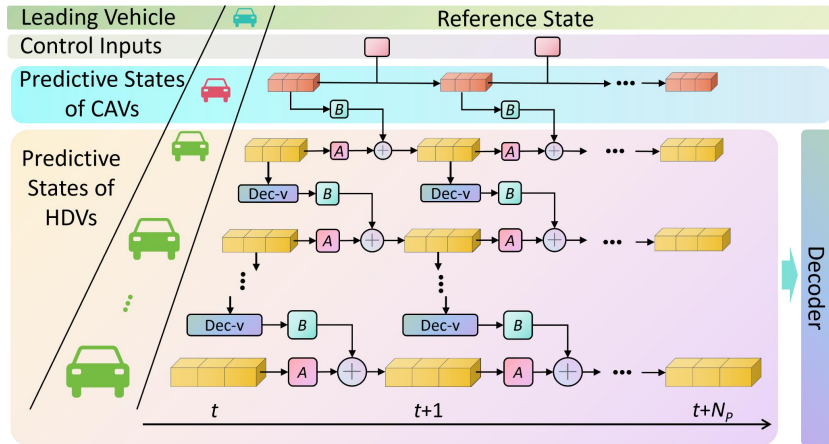


Figure 5: State Predictive Process of Mixed Traffic System

2 4.3. AdapKoopPC for mixed traffic system

3 4.3.1. Constrained optimization problem of mixed traffic system

4 Assuming the predictive horizon is the same as the control horizon and denoting it as N_P , at time t , the optimization
5 objective for the mixed traffic system defined in Section 4.1 can be formulated as minimizing the following cost function
6 over the horizon to find an optimal set of control inputs $U^*(t) = [U^*(0|t), U^*(1|t), \dots, U^*(N_P - 1|t)]^T$:

$$J = \sum_{i=1}^{N_P} \|ES(i|t) - ES_{ref}(t+i)\|_Q^2 + \|U(i-1|t)\|_R^2 \quad (29)$$

7 where $ES(i|t)$ is the predictive state of the system after time steps i at time t ; $ES_{ref}(t)$ represents the reference
8 state, it provides the reference values for the velocity of CAVs in the system, namely the average velocities of their
9 respective preceding vehicles over the time interval $t - N_P$ to t ; Q and $R = r_u \cdot I_G$ are diagonal matrices, representing
10 the penalty weights for state and control input, respectively, where Q contains penalties for velocities of CAVs and
11 velocity differences of HDVs, defined as follows:

$$Q = \begin{bmatrix} q_{CAV} & & & \\ & q_{HDV} & & \\ & & \ddots & \\ & & & q_{HDV} \end{bmatrix}, q_{CAV} = \begin{bmatrix} 0 & & \\ & q_{CAV}^v & \\ & & 0 \end{bmatrix}, q_{HDV} = \begin{bmatrix} 0 & & \\ & 0 & \\ & & q_{HDV}^{\Delta v} \end{bmatrix} \quad (30)$$

¹ Additionally, the system states and control inputs must satisfy the following constraints:

$$\begin{aligned} h_{\min} < h(t) < h_{\max} \\ v_{\min} < v(t) < v_{\max} \\ a_{\min} < a_{CAV}(t) < a_{\max} \\ u_{\min} < u(t) < u_{\max} \end{aligned} \quad (31)$$

² These constraints respectively imply that the headways of all vehicles in the system should remain within a reasonable range, velocities should stay within velocity limits, and the acceleration and control inputs of CAVs should adhere to vehicle dynamics constraints.

⁵ 4.3.2. Standard quadratic programming of AdapKoopPC

⁶ To facilitate solving, the constrained optimization problem of mixed traffic system can be reformulated as a standard
⁷ quadratic programming problem. Building on the linear model described in Eq.(25), the predictive states among the
⁸ future N_P steps can be expressed as:

$$ES(t) = AS(t) + BU(t) \quad (32)$$

$$\begin{aligned} \text{where } ES(t) = [ES(1|t)^T, \dots, ES(N_P|t)^T]^T; BU(t) = [U(0|t)^T, \dots, U(N_P-1|t)^T]^T; A = \begin{bmatrix} CA_S \\ \vdots \\ CA_S^{N_P} \end{bmatrix}^T, B = \\ \begin{bmatrix} C_S B_S & & & \\ C_S A_S B_S & C_S B_S & & \\ \vdots & \vdots & \ddots & \\ C_S A_S^{N_P-1} B & C_S A_S^{N_P-2} B & \dots & C_S B_S \end{bmatrix}^T. \end{aligned}$$

¹¹ Let $ES_{ref}(t) = [ES_{ref}(1|t)^T, \dots, ES_{ref}(N_P|t)^T]^T$, $Q = I_{N_P} \otimes Q$, $R = I_{N_P} \otimes R$, where \otimes is Kronecker
¹² product. And by discarding the terms without $U(t)$, the cost function Eq.(29) has been rewritten as follows:

$$J = \frac{1}{2} U(t)^T H U(t) + F^T U(t) \quad (33)$$

¹³ where $H = 2(B^T Q B + R)$; $F^T = 2(A S(t) - ES_{ref}(t))^T Q B$. Optimal control input sequence can be obtained by
¹⁴ solving the constrained optimization problem (33) subject to Eqs. (31) and (32).

¹⁵ 5. Experiment Part I: AdapKoopnet for car following trajectory prediction of HDVs

¹⁶ 5.1. Dataset description and evaluation metrics

¹⁷ The performance of AdapKoopnet model is evaluated on the HighD dataset, which is a large-scale naturalistic
¹⁸ vehicle trajectory dataset collected from German highways. The dataset comprises 11.5 hours of measurements and
¹⁹ covers 110,000 vehicles, with a total measured vehicle distance of 45,000 km, capturing trajectories of both passenger
²⁰ cars and trucks. The car-following trajectory dataset is extracted in accordance with the criteria presented in Mo et al.
²¹ (2021), includes eleven fields such as id, precedingId, xVelocity, xAcceleration, and precedingXVelocity, totaling
²² 18396432 records. And the root mean square error (RMSE) is selected as the evaluation metrics:

$$RMSE = \sqrt{\frac{1}{\Gamma} \sum_{i=1}^{\Gamma} (y_i - \bar{y}_i)^2} \quad (34)$$

1 5.2. Baseline models and experiment settings

2 The performance of designed AdapKoopnet for HDVs car following trajectory Prediction is compared and evaluated
3 with the following baseline models.

4 **MLP** utilizes a multi-layered nonlinear fully connected neural network to predict the car-following trajectory of vehicle.

5 **LSTM** utilizes LSTM-based encoder-decoder architecture to predict vehicle trajectories Park, Kim, Kang, Chung and
6 Choi (2018).

7 **Koopnet** is an ablation version of AdapKoopnet where the extraction of driving characteristics semantic information
8 from the trajectories context of vehicle is eliminated. This emphasizes the importance of the driving characteristic
9 extraction block.

10 **N-AdapKoopnet** is a variant of AdapKoopnet where the decoder is replaced with fully connected layers featuring
11 non-linear activation functions. This demonstrates the impact of linear decoder on the prediction results.

12 **N-Koopnet** is similar to N-AdapKoopnet, features an encoder composed of fully connected layers with non-linear
13 activation functions.

14 **S-AdapKoopnet** employs a modified architecture in which the width of each layer is halved compared to AdapKoopnet
15 while retaining the same structure. This modification aims to reduce the computational load, especially when
16 implementing optimization for large-scale mixed traffic systems.

17 PyTorch 2.1.0 framework is utilized to construct the predictive model, and end-to-end training was performed
18 under a platform with Intel Core i9-13900K processor and NVIDIA RTX 4090 GPU. The processed car-following
19 trajectories were split into training, validation, and test sets in a ratio of 7:1:2. The model relevant hyperparameters
20 are detailed in 1.

Table 1

Model hyperparameter

Hyperparameter Type	Hyperparameter	Values
Explicit State Encoder	Number of Layers	3
	MLP activation function	Tanh
	Dropout	0.2
Semantic Extraction Block	Trajectory Context horizon	31
	Driving Scenario type	3
	Attention head	4
	Attention dimension	64
	Input feature dimension	5
Other hyperparameters	Model dimension	128
	Prediction horizon	15
	Batch size	256
	Max train epochs	25
	learning rate(LR)	10^{-5}
	LR scheduler	Exponent
	LR decay rate	0.6

21 5.3. Trajectory prediction experiment results

22 5.3.1. HDVs trajectory prediction performance comparison

23 Table 2 statistics the performance index results of AdapKoopNet and other baseline models for trajectory prediction
24 under different prediction horizons, including the RMSE of velocity and headway. In terms of velocity, when
25 the prediction step is 5 (0.6 seconds), the RMSE of LSTM is the smallest at 0.084m. The reason may be due to the
26 architectural design of the LSTM encoder-decoder and the excellent gate control unit structure, which has advantages
27 in short time domain prediction. When the prediction step increases to 1.2 seconds, AdapKoopNet has a significant
28 advantage, with an RMSE of 0.145m, which means it has better long-term prediction ability. AdapKoopnet considers
29 the multi-step evolution loss of linear space during the training process, giving up some short-term prediction per-
30 formance in exchange for the average prediction performance in the entire prediction time domain. It is also worth
31 mentioning that although Koopman theory provides a global linear expression of a dynamic system in an infinite-
32 dimensional space, AdapKoopnet ultimately implements predictions in a finite-dimensional (128-dimensional) space,
33 which is bound to be affected by linear systems, resulting in some losses. Simply put, with the help of the powerful

1 feature extraction capability of the attention mechanism and the adaptive driving feature extraction architecture based
 2 on driving scenarios, the AdapKoopnet series models have achieved performance comparable to LSTM in terms of
 3 short-term prediction performance, and better than it in terms of long-term prediction performance.

4 Although as the prediction step further increases, N-AdapKoopNet outperforms AdapKoopNet in performance,
 5 reflecting the loss of prediction performance caused by the adoption of linear decoders, the average performance at
 6 each prediction step size is still the most outstanding for AdapKoopNet. Subsequently, comparing the distance between
 7 the front of the vehicle, the most effective models are LSTM and N-AdapKoopNet. However, the decoder of this model
 8 is non-linear and can indeed achieve good trajectory prediction results. However, it is also not suitable for subsequent
 9 CAVs prediction control. Taking into account the accuracy of trajectory prediction and the feasibility of subsequent
 10 control for real-time traffic flow optimization, it is evident that AdapKoopNet has significant advantages. In addition,
 11 in order to balance prediction performance and inference cost, the large-scale hybrid transportation system simulation
 12 experiment in Section 6.3 is based on S-AdapKoopnet.

Table 2

Comparison of HDVs longitudinal trajectory prediction performance indicators

Model	Velocity RMSE(m/s)				Headway RMSE (m)			
	0.6s	1.2s	1.8s	Average	0.6s	1.2s	1.8s	Average
MLP	0.184	0.341	0.472	0.3324	0.447	0.659	0.882	0.663
LSTM	0.084	0.173	0.367	0.208	0.444	0.628	0.797	0.623
Koopnet	0.176	0.318	0.444	0.313	0.468	0.672	0.883	0.674
N-AdapKoopnet	0.110	0.155	0.243	0.169	0.455	0.628	0.769	0.618
N-Koopnet	0.200	0.322	0.444	0.322	0.454	0.647	0.851	0.650
S-AdapKoopnet	0.105	0.148	0.247	0.167	0.477	0.651	0.796	0.641
AdapKoopnet	0.095	0.145	0.2471	0.162	0.466	0.643	0.792	0.634

13 Fig. 6 (a) shows the indicator line graph of AdapKoopNet and the baseline models under complete 15 prediction
 14 steps, where the red line represents AdapKoopNet. The comparison results are obvious, mainly including the following
 15 two aspects. Firstly, regardless of the prediction range, the AdapKoopNet model outperforms KoopNet, indicating
 16 that it effectively and accurately captures the underlying data features and achieving personalized driving behavior
 17 prediction. Secondly, as the prediction range increases, although the prediction performance of AdapKoopNet has
 18 declined, it still maintains accuracy and feasibility. The comparative analysis with the baseline models is similar to
 19 Table 2 and will not be further elaborated.

20 Fig. 6 (b) focuses specifically on the prediction step scene of 1.8s. 300 batches are randomly selected from the
 21 test set, and the predicted and true values of headway and velocity are visualized, with the color axis representing
 22 the probability density. It can be observed that the velocity of most trajectory appears between 20 and 30 meters,
 23 while the headway remains around 30 to 50 meters. In addition, the vast majority of trajectory samples are attached
 24 near the diagonal, which means that the predicted values are very close to the true values, reflecting the strong ability
 25 of AdapKoopNet to capture trajectory evolution features and make accurate predictions. Of course, there are some
 26 samples with significant deviations, but it can be seen that these scattered points are all dark blue, indicating that the
 27 density of these samples is extremely low and almost does not affect the overall trajectory prediction performance.
 28 Of course, benefiting from the rolling optimization method adopted in the AdapKoopPC, the negative impact of these
 29 deviation samples on the subsequent mixed traffic flow optimization control can be ignored.

30 **5.3.2. Potential scenarios recognition and clustering results**

31 Furthermore, in order to verify the effectiveness of AdapKoopnet in directly extracting potential driving scenarios
 32 from real trajectory data and adaptively learning driving characteristics without any pre-define or pre-label, a series of
 33 visualizations of the model training results are performed.

34 The first thing to explore is what all trajectory samples output after passing through the multi-head driving scenario
 35 recognition module. Fig. 7 shows the distribution of trajectory samples for various driving scenarios learned and
 36 clustered. Fig. 7 (a), (b) and (c) show the headway-velocity relationship of trajectory samples under three driving
 37 scenarios. The color axis represents the proportion of samples, with the proportion of trajectory samples increasing as
 38 the color approaches red. It is obvious that Fig. 7 (a) tends towards medium to high velocity driving scenario, with the
 39 highest proportion of sample clusters distributed at velocity of around 25m/s, accompanied by a moderate headway of

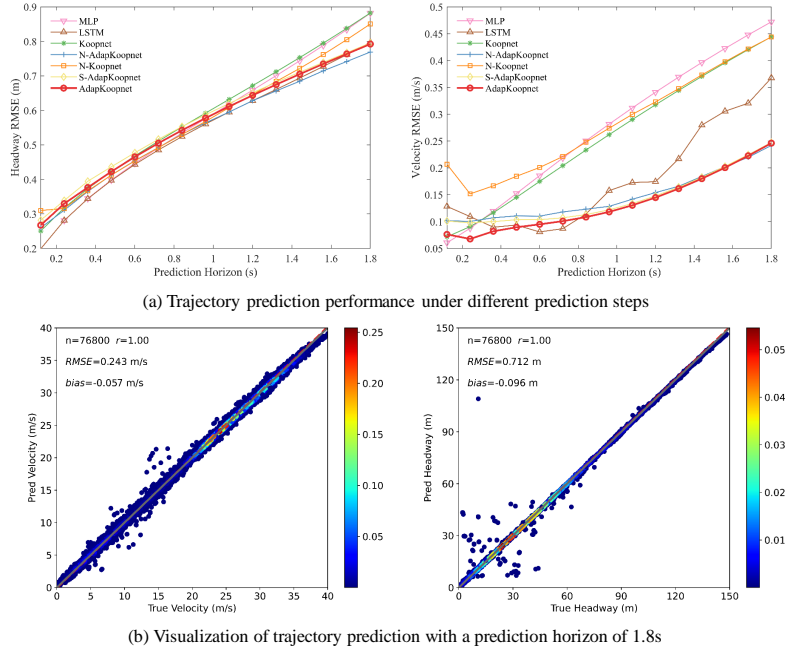


Figure 6: HDVs driving state prediction performance of the AdapKoopnet

1 30 meters to 60 meters. The distribution of trajectory samples in Fig. 7 (b) is relatively uniform, including scenario
 2 with small headway at low velocity and large headway at high velocity. Fig. 7 (c) corresponds to the third driving
 3 scenario, where the overall trajectory exhibits low velocity accompanied by small headway. Fig. 7 (d), (e), and (f)
 4 depicts the relationship between the average velocity difference, average headway, and average velocity of trajectory
 5 samples in three driving scenarios, with the color axis representing velocity. Significantly, all trajectory samples are
 6 clearly clustered into three driving scenarios, each with similar repetitive patterns. Of course, the characteristics of
 7 all trajectories in each posture scenario are not entirely the same. Overall, AdapKoopNet has the ability to adaptively
 8 extract features from a large number of trajectory samples and cluster them, ultimately forming these three potential
 9 driving scenarios.

10 5.3.3. Scenario inherent temporal correlation and the driving characteristics dynamic temporal correlation

11 Fig. 8 reveals this specific driving scenario inherent temporal correlation and the driving characteristics dynamic
 12 temporal correlation. Fig. 8 (a) corresponds to the output of the driving characteristics semantic module shown in 3 (b)
 13 in AdapKoopNet. It is worth noting that as mentioned earlier, AdapKoopNet adaptively learns the feature weights of
 14 each trajectory sample belonging to three different scenarios, and then clusters them into potential scenarios according
 15 to their propensity. Therefore, more precisely, what is extracted here is the inherent temporal correlation corresponding
 16 to each driving scenario. Specifically, driving scenario 1 and driving scenario 3 are quite similar, both reflecting an
 17 overall trend of lower temporal correlation as the historical time step increases. The difference lies in that the former
 18 is not as extreme as the latter, and Scenario 3 strongly relies on the nearest time step and has almost no correlation on
 19 distant historical trajectories. There is a significant difference between driving scenario 2 and the above two driving
 20 scenarios, characterized by a more stable temporal correlation on the historical trajectory of each time step, rather than
 21 being more affected as time approaches.

22 Fig. 8 (b) indicates the dynamic correlation that directly reflects the actual driving characteristics of each vehicle.
 23 Here, we visualized six vehicles trajectories in each scenario. Significantly, whether it is driving scenarios 1,
 24 2, or 3, the corresponding six trajectories exhibit dynamic correlations equivalent to the six variants in each driving
 25 scenario. They tend towards a scenario and follow the inherent temporal characteristics of the driving scenario, but
 26 the driving characteristics of each trajectory are different from each other, corresponding to the driving characteristic

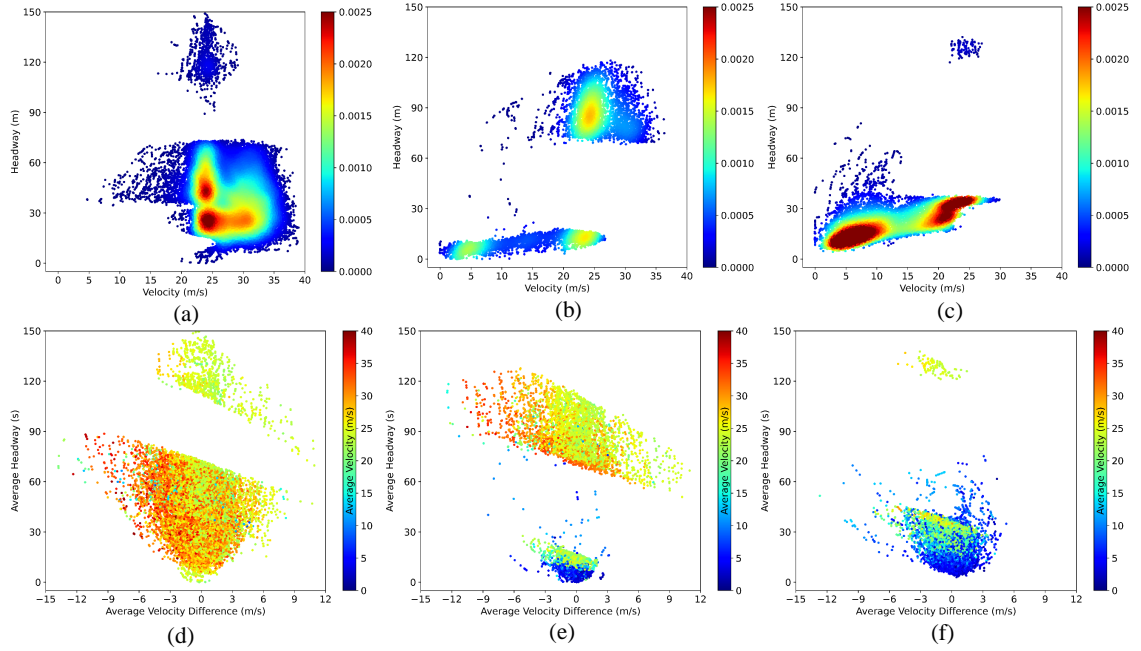


Figure 7: Adaptive Multi-driving scenario recognition results

dynamic correlation module. These indeed demonstrate that AdapKoopNet has adaptively learned the inherent temporal correlations and driving characteristics dynamic correlations in different driving scenarios. The capture of these correlations contributes to subsequent accurate and personalized trajectory prediction, which is elaborated and proven in the following section.

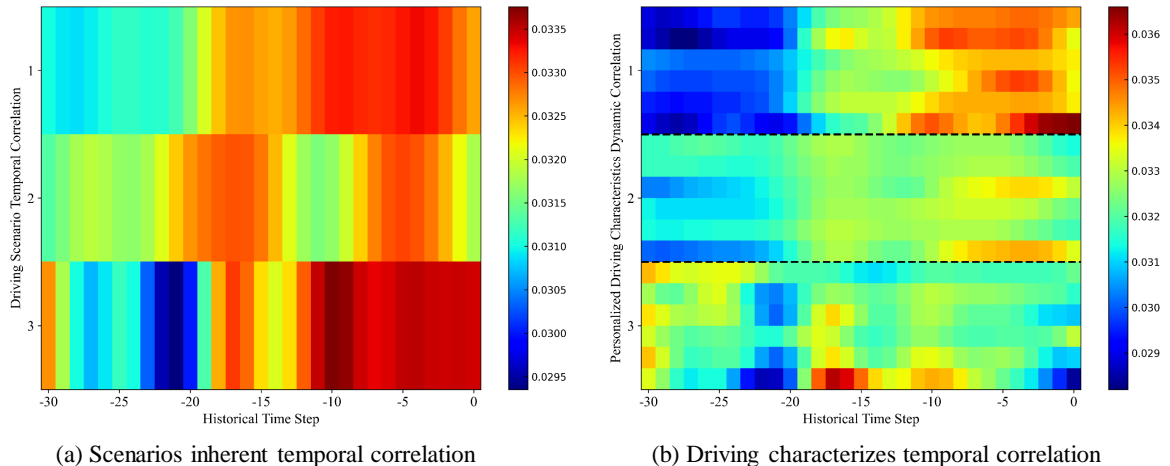


Figure 8: The inherent temporal correlation of driving scenarios and the temporal correlation of driving characteristics

1 **5.3.4. Validation of scenarios recognition effectiveness**

2 Fig. 9 is a comparative experiment demonstrating the effectiveness of the multi-head driving scenario recognition
3 module and the driving characteristics semantic transformation module in learning potential driving scenarios and
4 dynamic temporal correlation. Two trajectory test samples were selected, corresponding to adaptive learning of three
5 driving scenario characteristic weight of 0.012:0.020:0.968 and 0.330:0.151:0.519, corresponding to Fig. 9 (a) and
6 Fig. 9 (b), respectively. A very direct and convincing approach is to manually input different driving scenario labels
7 for the same trajectory, and then compare its trajectory prediction results with those of unlabeled adaptive learning.
8 Firstly, as shown in Fig. 9 (a), the feature weight of driving scenario 3 is 0.968, which is almost close to 1. The
9 predicted trajectory with manually labeled scenario 3 is almost completely consistent with the trajectory prediction
10 results with unlabeled adaptive learning, while the trajectory prediction results in manually labeled driving scenarios 2
11 and 3 are significantly different. The predicted velocity parameters of the trajectory show the same comparative results.
12 By comparison, Fig. 9 (b) shows that the feature weight of driving scenario 3 learned by AdapKoopNet is 0.519, and
13 the trajectory features are more inclined towards scenario 3. It is obvious that in both headway and velocity aspects,
14 the trajectory prediction results for scenario 3 with manual label driving represented by the yellow line, closely align
15 with the observed values, followed by scenario 1 with manual label, and scenario 2 with manual label has the largest
16 trajectory prediction deviation. The above comparison serves as strong evidence of the effectiveness and superiority of
17 AdapKoopNet. In addition, there is actually another discovery that as the prediction step size increases, the prediction
18 trends under various preset conditions are similar in trajectory prediction. This phenomenon arises from the fact that
19 different prediction conditions correspond to different Koopman operators, with the only variation being the associated
20 feature vectors. This is worth further improvement in future research.

21 **6. Experiment Part II: AdapKoopPC for mixed traffic system**

22 This section aims to comprehensively evaluate the effectiveness and superiority of the proposed AdapKoopPC in
23 mitigating traffic oscillations in mixed traffic flows. Specifically, it covers small-scale experiments and large-scale
24 experiments. The former aims to compare the spatio-temporal evolution trajectory of each vehicle in the mixed traffic
25 system based on AdapKoopPC and based on other benchmark control methods, see Section 6.2; the latter is to verify
26 the application of AdapKoopPC for the performance and generalization ability of large-scale mixed transportation
27 systems, see Section 6.3.

28 **6.1. Simulation settings**

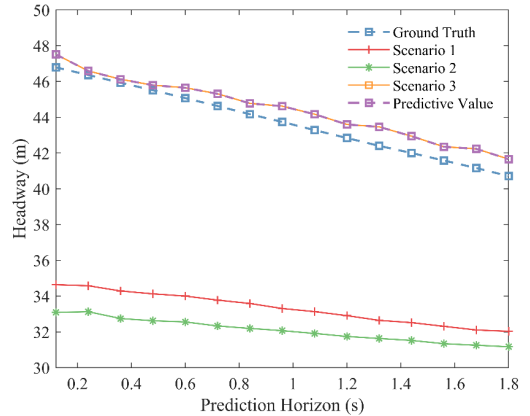
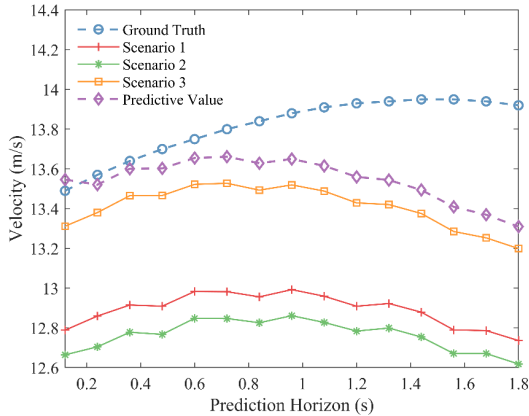
29 The small-scale simulated mixed traffic system consists of 2 CAVs, 2 HDVs(Truck) and 6 HDVs(Car). The large-
30 scale simulated mixed traffic system consists of 50 vehicles, of which CAVs and HDVs(Car) account for 80%, and
31 HDVs(Truck) account for 20%. A certain proportion of trucks is set up to build a heterogeneous simulation environ-
32 ment, with the purpose of proving the modeling and prediction capabilities of AdapKoopPC for heterogeneous HDVs.
33 IDM is used as the simulation control model of HDVs, and its parameters are calibrated and obtained from the natu-
34 ralistic driving dataset using genetic algorithm. The simulation is conducted on an open road, and the head vehicle of
35 the mixed traffic system evolves according to the following equation to simulate traffic oscillations Ruan, Wang, Zhou,
36 Zhang, Dong and Zuo (2022):

$$v_0(t) = \begin{cases} 25 \text{ m/s} & t \in [0, 4.8] \text{ s} \\ 25 - 5 \sin(0.1667(t - 4.8)) \text{ m/s} & t \in [4.8, 180] \text{ s} \end{cases} \quad (35)$$

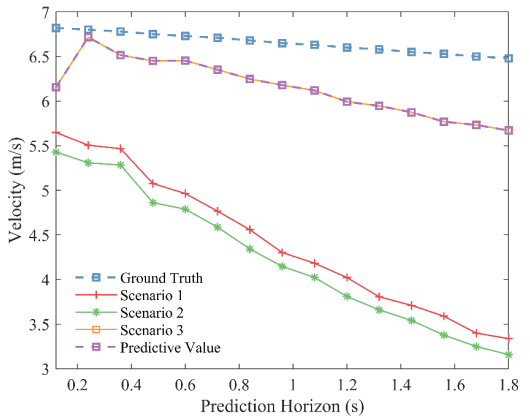
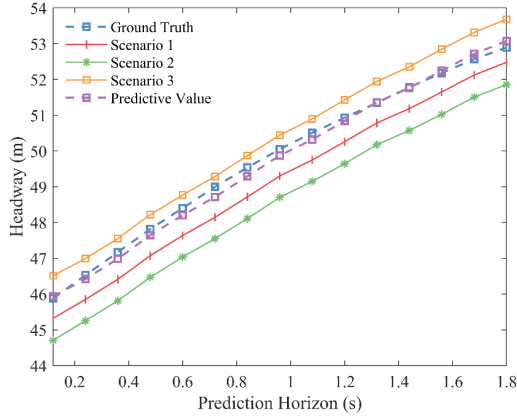
37 Except for the first vehicle, which must be a CAV, the arrangement of vehicles in the system is randomly generated
38 based on the proportion of vehicle types. The control input for CAVs is solved using the SLSQP optimizer from the
39 Scipy library, and the simulation is conducted on a laptop equipped with the Apple M2 chip. The simulation experiment
40 parameters are shown in Table 3.

41 **6.2. Real-time control optimization experiment for small-scale mixed traffic system**

42 The Small-scale experiment aims to validate the effectiveness of AdapKoopnet in balancing traffic flow distur-
43 bances and enhancing traffic flow stability, as well as the computational efficiency. The baseline control methods
44 including:



(a) Driving scenario learning feature weight with 0.012:0.020:0.968



(b) Driving scenario learning feature weight with 0.330:0.151:0.519

Figure 9: Trajectory prediction results for the same trajectory under different driving scenario

Table 3

Parameter settings for comparative experiments with different control methods

	Parameter	Value	Parameter	Value	Parameter	Value
IDM	a_{IDM}^{car} (m/s^2)	1.13	a_{IDM}^{truck} (m/s^2)	1.5	v_{IDM}^{car} (m/s^2)	35.96
	b_{IDM}^{car} (m/s^2)	4	b_{IDM}^{truck} (m/s^2)	4	v_{IDM}^{truck} (m/s^2)	54.25
	s_0^{car} (m)	8.16	s_0^{truck} (m)	9.66	l^{car} (m)	4.24
	T_0^{car} (m)	1.13	T_0^{truck} (m)	1.72	l^{truck} (m)	11.82
AdapKoopPC	h_{\min} (m)	20	v_{\min} (m)	0	a_{\max} (m/s^2)	6
	h_{\max} (m)	150	v_{\max} (m)	150	a_{\min} (m/s^2)	-6
	u_{\min} (m/s^3)	-6	u_{\max} (m/s^3)	6	N_p	10
	$q_{HDV}^{\Delta v}$	20	q_{CAV}^v	10	r_u	2
Simulation	Duration(s)	180	Interval(s)	0.12	Truck proportion	20%

¹ **LTI-MPC**: On the premise that the car-following model adopted by HDVs in the mixed traffic system is known, linear time-invariant MPC is used to optimize the mixed traffic system based on the linearized car-following model Wang et al. (2023a).

⁴ **Deep-LCC**: A data-driven non-parametric predictive control framework for mitigating traffic flow velocity oscillations.

⁵ And the evolution dynamics of mixed traffic systems are learned online using the pre-collected trajectories Wang et al. (2023a).

1 Additionally, to make a sound comparison of the proposed AdapKoopPC with the baselines, a fixed random seed
2 is setting in the small-scale simulation.

3 **6.2.1. Mixed traffic system evolution results**

4 Fig. 10 and Fig. 11 depict and compares the headway and acceleration evolution of small-scale mixed traffic system
5 under different control methods. The yellow dashed line represents the head vehicle, while the blue and orange thick
6 solid lines represent the two CAVs under various control methods. The remaining 8 vehicles are all HDVs, with HDV8
7 and HDV10 being trucks and the rest being cars. Fig. 10 (a) and Fig. 11 (a) depict the evolution of the mixed traffic
8 system corresponding to no control, where the CAV solely considers optimizing its following trajectory with respect to
9 the head vehicle, without taking into account its own guiding influence on the subsequent HDVs. After the head vehicle
10 experiences disturbances starting at 4.8s and begins to oscillate, and the entire system exhibits substantial acceleration
11 and deceleration. The evolution of the blue line in the middle subgraph indicates that as the CAV decelerates with the
12 leading vehicle, the velocity of the entire mixed traffic system also begins to oscillate significantly. The following HDVs
13 exhibit significant fluctuations in their headways. Taking the first HDV following behind as an example, the headway
14 drops to 33 meters and then continues to rise to around 72 meters, indicating poor stability due to the promotion of
15 disturbances through the entire system.

16 Fig. 10 (b) and Fig. 11 (b) shows the mixed traffic system evolution after implementing the LTI-MPC. There is
17 a change that needs to be explained in advance, which is that the first CAV did not maintain a constant velocity with
18 the leading vehicle at the beginning. This is because LTI-MPC imposes a penalty on the error between the actual
19 headway and the expected headway. Once there is a small error between the initial headway set in the experiment and
20 the expected headway after traffic system operates, it will lead to fluctuations in the initial stage of mixed traffic system
21 evolution, which is difficult to be avoided in the experimental setup. It is obvious that the amplitude of the velocity
22 oscillation of the first CAV also begins to oscillate after receiving the oscillation propagation from the leading vehicle,
23 and the following HDV also oscillates with it. The overall oscillation amplitude decreases relative to Basic-MPC. In
24 terms of headway, taking the second HDV indicated by the red line as an example, the oscillation amplitude of the
25 headway improved due to the influence of the CAV ahead, reaching a maximum front distance of about 50 meters at
26 40 seconds. Subsequently, the second CAV also optimized its driving behavior under the action of LTI-MPC, and the
27 trajectories of the following two trucks also fluctuated accordingly, maintaining a distance near the expected headway.

28 The evolution and improvement of the mixed traffic system under the Deep-LCC control scenario are shown in
29 Fig. 10 (c) and Fig. 11 (c). Similarly, the initial evolution stage, like the LTI-MPC, requires the first CAV to accelerate
30 in order to achieve equilibrium headway. We can clearly observe that there is little difference between Deep-LCC
31 and LTI-MPC in overall traffic system evolution improvement, achieving performance comparable to LTI-MPC. The
32 specific details will not be repeated in the description. Of course, Deep-LCC does not require prior knowledge of
33 system dynamics, and its advantage lies in its data-driven non parametric strategy.

34 To shift the perspective shifts to Fig. 10 (d) and Fig. 11 (d), the figures show how the mixed vehicle latoon
35 trajectory evolves under AdapKoopPC control. In terms of acceleration, the CAV perceives the oscillation of the
36 leading vehicle and begins to slow down slightly, then maintains a small amplitude of acceleration and deceleration
37 driving behavior, and induces the vehicles behind to maintain a small amplitude of acceleration and deceleration driving
38 behavior. The acceleration evolution is noticeably improved compared to the previous scenario, with the fluctuation
39 range around -0.25m/s to 0.25 m/s. In terms of headway, the headway of CAV is relatively large compared to other
40 previous control methods, but it ensures that the oscillation of the rear HDV headway is significantly reduced, from
41 the previous 30-60 meters to 40-50 meters. This is direct evidence that AdapKoopPC effectively proactively guides
42 and optimizes subsequent HDV driving behavior. It is worth mentioning that the headways of the two trucks after the
43 second CAV fluctuates smoothly and is almost unaffected by the disturbance of the leading vehicle.

44 Overall, these comparative results further demonstrate that AdapKoopPC can effectively and proactively guide
45 the subsequent HDVs and maintains the smooth driving of the mixed traffic system. More importantly, whether it is
46 LTI-MPC or Deep-LCC, it is necessary to utilize a given model or simulation to generate some trajectories. However,
47 these trajectories are highly dependent on the expected headway, which has limitations. AdapKoopPC adopts a penalty
48 of velocity difference, which matches the expected goal of most drivers of vehicles in a following state. This will not
49 cause discomfort to the driver and is more conducive to optimize the control of the mixed traffic flow system.

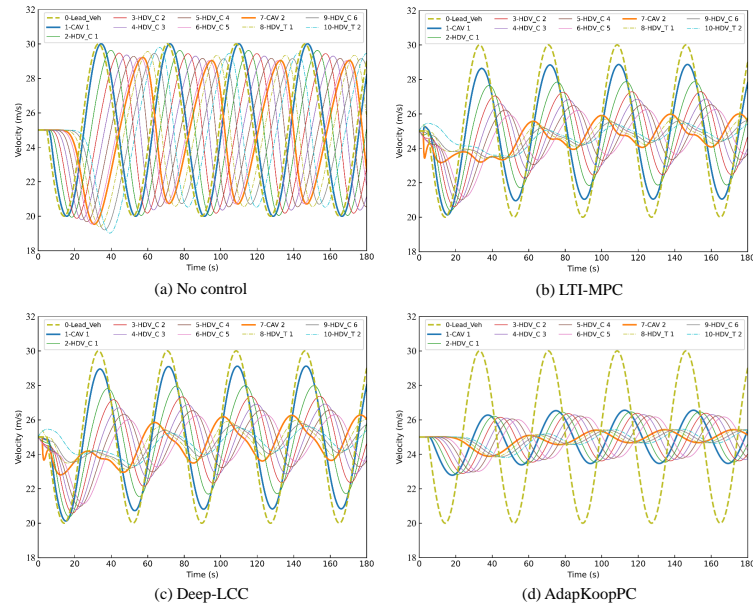


Figure 10: The mixed traffic flow velocity evolution comparison under different control methods

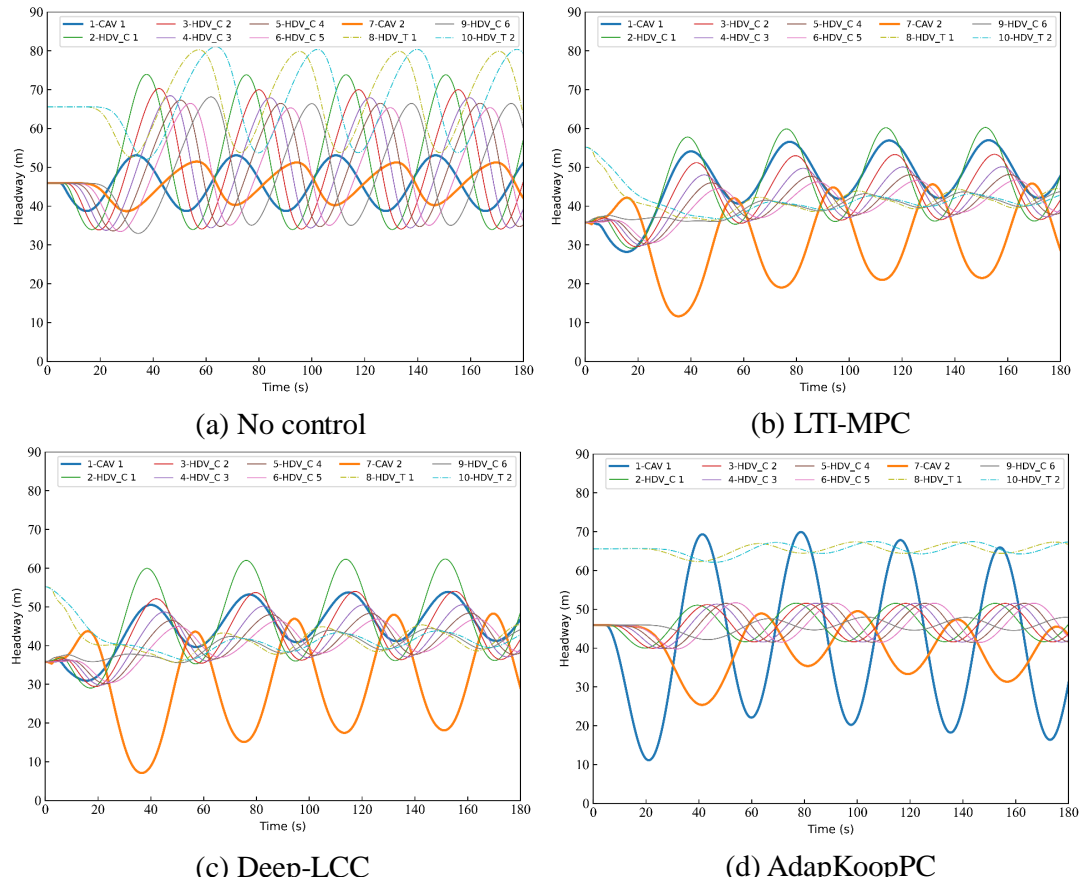


Figure 11: The mixed traffic flow headway evolution comparison under different control methods

1 **6.2.2. Computation time comparison**

2 Table 4 states the real-time computing time for different control methods at each time step, with a time step of 0.12
3 seconds. The average computation time for LTI-MPC, Deep LCC, and AdadKoopPC is 0.004s, 0.326s, and 0.009s,
4 respectively. To investigate its reasons, LTI-MPC does not require neural network encoding, and the mixed traffic
5 system state dimension is low, so the solution is the fastest. As for Deep-LCC, it was shown to be 0.05s in the previous
6 work. The online computation time of Deep-LCC has shown significant fluctuations in our experiments. When simu-
7 lating mixed traffic flow system scenarios similar to pre-generated trajectory scenarios, the average computation delay
8 is 0.326 seconds. When there is a significant difference between the two scenarios, the model training solution needs
9 to iterate to the maximum number of manually set iterations. Therefore, the delay depends on this value and will not
10 be lower than 0.326 seconds, which may be due to a lack of generalization ability. After the impact of neural network
11 encoding time and significant increase in state dimension, the online computation of AdadKoopPC yields an average
12 time of 0.009 seconds, and the sampling interval is 0.12 seconds, which demonstrates the feasibility of implementing
13 real-time mixed traffic system control. It is worth mentioning that the simulation experiments of LTI-MPC and Deep-
14 LCC are based on the MATLAB quadprog optimizer, which has better solving performance compared to the SciPy
15 adopted in AdadKoopPC. Therefore, the online computation time of AdadKoopPC can still be further improved.

Table 4
Computation Time

Model	LTI-MPC	Deep-LCC	AdadKoopPC
Computing Time (s)	0.004	0.326	0.009

16 **6.3. Real-time control optimization experiment for large-scale mixed traffic system**

17 This section verifies the effectiveness and strong generalization ability of AdadKoopPC for large-scale mixed traffic
18 system control, where the leading vehicle is followed by 50 vehicles. Three types of traffic flow scenarios covering
19 different CAVs penetration rates, communication range degradation, and different CAVs distribution are set up to
20 analyze the effectiveness and performance loss of AdadKoopPC in traffic flow optimization control in a wide range of
21 scenarios.

22 **6.3.1. CAVs penetration rates**

23 Fig. 12 depicts the overall evolution of the mixed vehicle with AdadKoopPC under different CAV penetration rates
24 in the large-scale mixed traffic system scenario, including 0%, 10%, and 20%. The horizontal axis represents time, the
25 vertical axis represents vehicle position, and the color axis represents velocity. Note that there are some white spacing
26 lines, indicating that the trajectory here is a truck trajectory with a greater headway than the headway of the car. The
27 following row shows the corresponding three-dimensional evolution diagram. The experimental comparison results
28 can be mainly summarized into the following two points: a) When there is no CAV in the traffic system, the disturbance
29 of the leading vehicle propagates directly upstream with the traffic wave, which can be reflected by the increasingly
30 prominent red area in Fig. 12(a). The three-dimensional velocity evolution diagram provides a more intuitive view
31 of the poor driving conditions of the traffic system. b) As the penetration rate increases to 10%, the traffic wave
32 gradually dissipates and there is no significant fluctuation in the velocity of following vehicles. Until the penetration
33 rate reaches 20%, the velocity oscillation can be almost ignored and maintained around the expected velocity of 25m/s.
34 An experiment with the 30% penetration rate has also been conducted, and its effect is very close to that of 20%, which
35 is not shown here. It can be considered that the effect is approaching saturation at 20% penetration rate. Overall,
36 AdadKoopPC has the ability to significantly alleviate upstream disturbance waves.

37 **6.3.2. Communication range degradation**

38 Another special case has also been considered, where CAV deteriorates within communication range due to external
39 factors. The vehicle can only receive information from the following vehicle, and cannot obtain the driving states of
40 all vehicles. And the performance degradation of AdadKoopPC in this scenario is investigated ,the results are shown
41 in Fig. 13. Note that more communication restricted scenarios fall between the communication degradation scenario
42 discussed here and the communication lossless scenario, so the control effect of AdadKoopPC in other scenarios will
43 be better than the extreme scenario presented below.

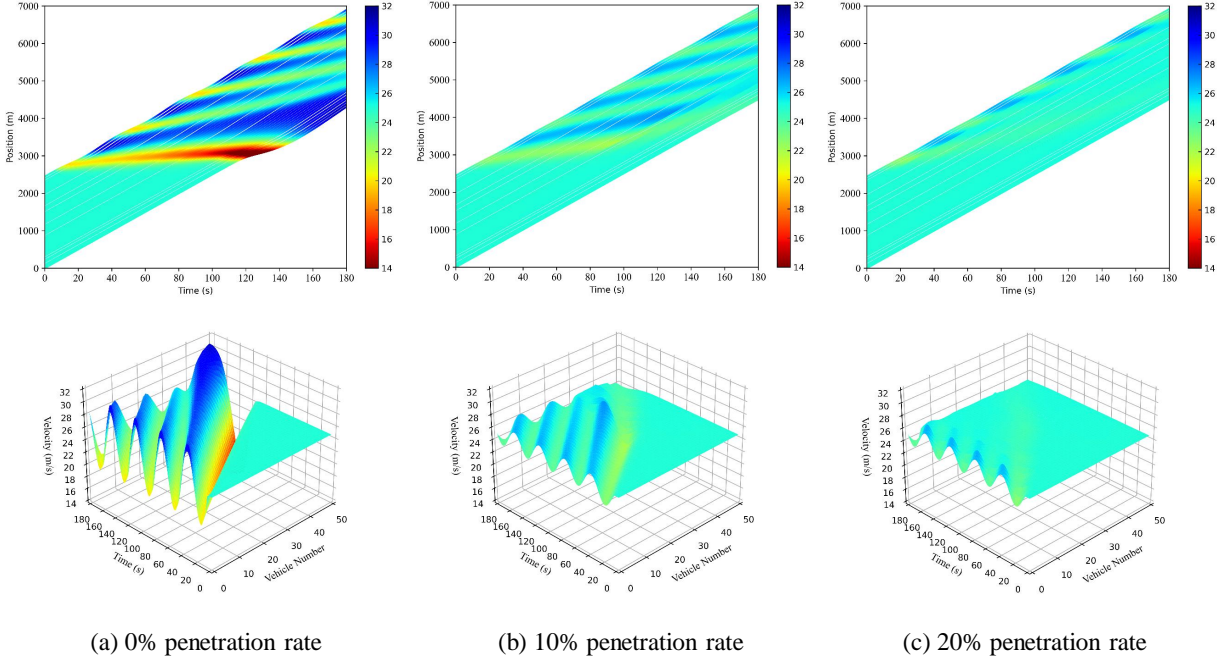


Figure 12: The mixed traffic flow evolution with AdapKoopPC under different CAVs penetration rates

Three penetration rates of 10%, 20%, and 30% are set for experiments under the premise of communication range degradation. Firstly, by comparing Fig. 13 (a) with Fig. 12 (a), AdadKoopPC still plays a significant role, and the traffic oscillation wave generated by the leading vehicle is significantly alleviated. Secondly, the difference between Fig. 13 (a) and Fig. 12 (b) intuitively reflects the impact of communication range degradation on the overall evolution improvement of the traffic system. The oscillation slightly increases, indicating that the performance of AdadKoopPC has been slightly degraded. Similarly, in the scenario of a 20% penetration rate, due to the impact of communication range degradation on AdadKoopPC, CAV only considers optimizing and inducing the first vehicle behind it, resulting in a decrease in the overall mixed traffic system evolution effect, which can be observed by comparing Fig. 13 (b) and Fig. 12 (c). Of course, under the above two penetration rates, even if the communication range is degraded, the traffic system oscillation propagation is still within an acceptable range, proving that AdadKoopPC can still induce and optimize the performance of the entire system even under the influence of communication range degradation. Fig. 13 (c) corresponds to a 30% penetration rate. The simulation results confirm that the evolution of the traffic system is stable and smooth, and the optimization effect is approaching saturation.

6.3.3. CAVs distribution

To compare the control performance of AdapKoopPC in mitigating traffic oscillations under different CAV distributions in the mixed traffic flow, the arrangements of HDVs and CAVs are randomly generated while maintaining a fixed CAV penetration rate of 10%. Fig. 14 aims to explore the impact of AdapKoopPC on alleviating traffic oscillations under different CAV distributions. Fig. 14 (a) corresponds to a scenario where three CAVs are concentrated in the front of the mixed traffic flow, and its optimization effect on the mixed traffic flow is very close to Fig. 12 (c). This is related to the fact that CAVs in the front of the mixed traffic flow can eliminate oscillations almost without affecting subsequent vehicles. Fig. 14 (b) and Fig. 14 (c) correspond to the concentration of CAVs in the middle and rear of all vehicles, respectively. It can be observed that the effect is not as good as when CAVs are located in the front, which is understandable. Yet, the overall disturbance mitigation effect is significant. Additionally, an interesting finding is that when CAVs are more evenly distributed, the mitigation performance is better than when they are concentrated in the middle or rear. Overall, regardless of the position of the CAVs, AdapKoopPC performs well, fully demonstrating its effectiveness and universality, strong generalization ability, and suitability for various scenarios.

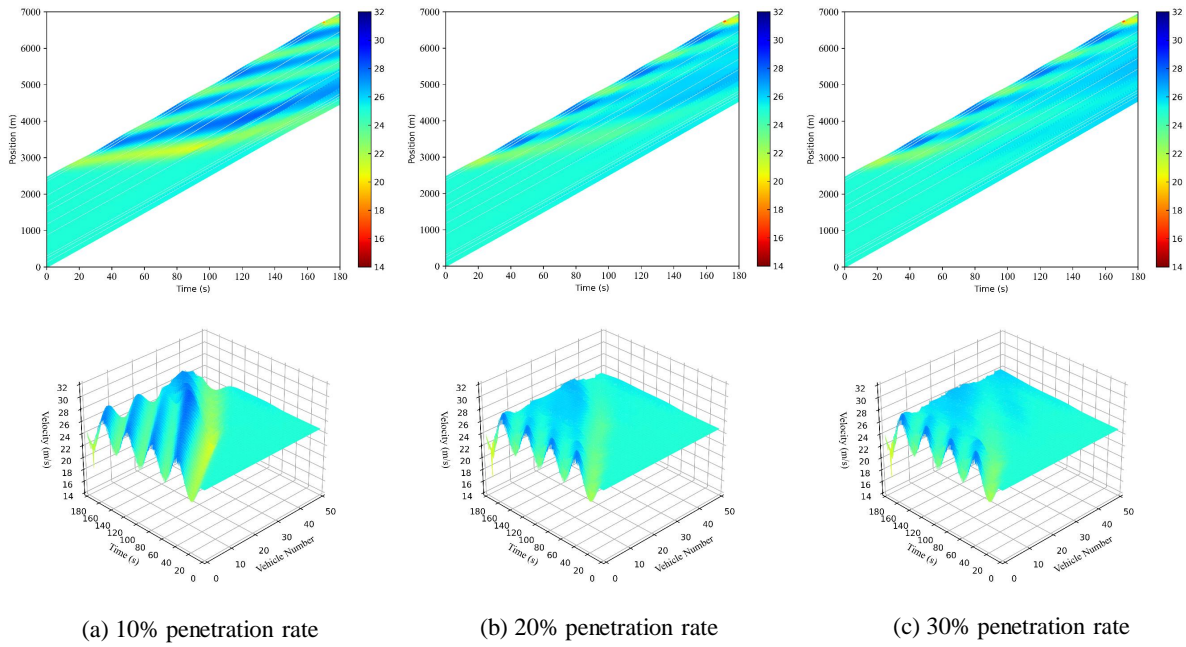


Figure 13: The mixed traffic flow evolution with AdapKoopPC under communication range degradation

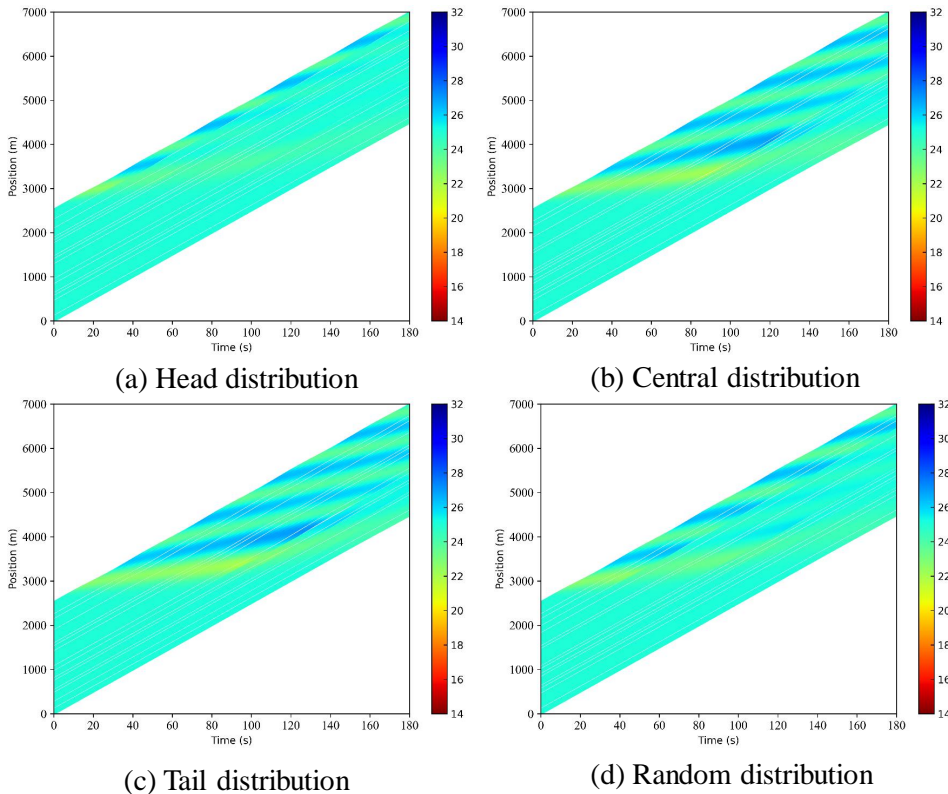


Figure 14: The mixed traffic flow evolution with AdapKoopPC under different CAVs distribution

Table 5

The impact of the number of controllers on reducing traffic flow oscillations

Number	v_{std} (m/s)	h_{std} (m)	Number	v_{std}	h_{std} (m)
0	3.30	8.34	1	2.28	5.55
2	2.18	5.47	3	2.16	5.65
4	2.07	5.48	5	2.04	5.55
6	1.85	4.85	7	1.84	4.86
8	1.65	4.15	9	1.61	3.99
10	1.61	3.98	11	1.59	3.92
12	1.60	3.94	13	1.58	3.89
14	1.58	3.88	15	1.58	3.89
16	1.59	3.86	17	1.59	3.84
18	1.59	3.83	19	1.59	3.83
20	1.59	3.81	/	/	/

6.3.4. Number of controller deployments

We further investigate how many CAVs are required to deploy the proposed AdapKoopPC controller in random conditions to achieve a satisfactory level of traffic flow improvement. A mixed traffic flow consisting of 20 CAVs and 30 HDVs were randomly generated, where the AdapKoopPC was randomly deployed on the CAVs. In order to quantitatively analyze the traffic flow improvement, the velocity standard deviation and headway standard deviation of all vehicles in the mixed traffic flow are used as evaluation indicators. The results are shown in Table 5. Overall, as the number of deployed controllers increases, the standard deviation of speed and headway gradually decreases. More importantly, the standard deviation of speed and headway achieves convergence when the controller was 15 in such a mixed traffic flow. At such situation, the speed oscillation was reduced by 52.12%, and the standard deviation of the headway was reduced by 53.36%.

7. Conclusions

The main challenge currently faced by optimizing mixed traffic systems through CAVs is to accurately recognize and predict the driving behavior of HDVs while meeting real-time online computing capabilities. The Koopman operator theory and extended dynamic mode decomposition can achieve the linear approximation of nonlinear dynamic systems in high-dimensional space, providing feasible solutions for current issues. In this study, we innovatively propose AdapKoopnet to realistically describe and predict the HDVs driving behavior in complex scenarios. Furthermore, the AdaptKoopPC within a predictive control framework is developed to optimize real-time control of mixed traffic systems. AdapKoopnet has the capability to adaptively cluster potential driving scenarios and extract driving features from HDVs historical trajectories, which are then fused with the explicit state of the vehicle to form a high-dimensional representation of the state. The AdapKoopPC integrates AdapKoopnet and benefits from its linear characteristics, to achieve more efficient real-time control of CAVs in mixed traffic flow systems. Subsequently, trajectory prediction and traffic flow control optimization experiments are conducted, and the following conclusions are mainly drawn:

1. Benefiting from the Koopman theory, the multi-step prediction performance of AdapKoopnet based on linear space surpasses LSTM-based nonlinear encoder-decoder of the same dimension. And the semantic extraction of trajectory context plays an indispensable positive role in the accuracy of HDVs state prediction;
2. With the excellent architecture and loss function design of AdapKoopnet, it possesses powerful trajectory clustering and scenario recognition capabilities without pre-label, as well as adaptive driving characteristics extraction capabilities;
3. AdaptKoopPC does not rely on prior HDVs car following models or pre-collected simulation trajectories, and has better scenario generalization ability. In small-scale mixed traffic flow experiments, AdapKoopPC has shown promising results in slowing down traffic disturbance oscillations and improving traffic system stability. Compared with baseline models, it has more satisfactory computational efficiency and practical application potential;
4. The large-scale experimental results show that when the penetration rate of CAVs is 20%, the inhibitory effect of AdapKoopPC on oscillations is close to saturation. In addition, in the case of communication degradation, the control effect of AdapKoopPC with 20% CAV penetration rate is roughly equivalent to that of a 10% CAV penetration rate in a V2X environment without communication loss; Moreover, the control effect of AdaptKoopPC varies under different CAVs distributions, yet consistently exhibit superior performance in all cases.

1 There are some limitations of this study. For example, Koopman operator and does not support online updates. And
2 AdapKoopPC still faces dimensional disasters when applied to ultra large scale mixed traffic flow system. In future
3 work, the online learning and efficient distributed control framework will be developed. Furthermore, expanding the
4 application scenario of AdapKoopPC to multiple lanes is also worth further exploration.

5 Acknowledgement

6 This research was supported by the project of the National Key R&D Program of China (No. 2023YFB4302701),
7 the National Natural Science Foundation of China (No. 51925801, 52232012, 52272343) and Natural Science Foun-
8 dation of Jiangsu Province (No.BK20221467).

9 References

- 10 Ahmadian, A., Bahrami, S., Nourinejad, M., Yin, Y., 2025. Investment and financing of roadway digital infrastructure for automated driving.
11 Transportation Research Part B: Methodological 192, 103146.
- 12 Alanazi, F., 2023. A systematic literature review of autonomous and connected vehicles in traffic management. Applied Sciences 13, 1789.
- 13 Avila, A.M., Mezić, I., 2020. Data-driven analysis and forecasting of highway traffic dynamics. Nature communications 11, 2090.
- 14 Ba, J.L., Kiros, J.R., Hinton, G.E., 2016. Layer normalization. arXiv preprint arXiv:1607.06450 .
- 15 Bando, M., Hasebe, K., Nakanishi, K., Nakayama, A., 1998. Analysis of optimal velocity model with explicit delay. Physical Review E 58, 5429.
- 16 Bansal, P., Graham, D.J., et al., 2023. Congestion in cities: Can road capacity expansions provide a solution? Transportation Research Part A: Policy and Practice 174, 103726.
- 17 Cui, S., Cao, F., Yu, B., Yao, B., 2021. Modeling heterogeneous traffic mixing regular, connected, and connected-autonomous vehicles under
18 connected environment. IEEE Transactions on Intelligent Transportation Systems 23, 8579–8594.
- 19 Dauphin, Y.N., Fan, A., Auli, M., Grangier, D., 2017. Language modeling with gated convolutional networks, in: International conference on
20 machine learning, PMLR. pp. 933–941.
- 21 Dey, K.C., Yan, L., Wang, X., Wang, Y., Shen, H., Chowdhury, M., Yu, L., Qiu, C., Soundararaj, V., 2015. A review of communication, driver
22 characteristics, and controls aspects of cooperative adaptive cruise control (cacc). IEEE Transactions on Intelligent Transportation Systems 17,
23 491–509.
- 24 Du, Y., Makridis, M.A., Tampère, C.M., Kouvelas, A., ShangGuan, W., 2023. Adaptive control with moving actuators at motorway bottlenecks
25 with connected and automated vehicles. Transportation research part C: emerging technologies 156, 104319.
- 26 Durrani, U., Lee, C., 2024. A new car-following model with incorporation of markkula's framework of sensorimotor control in sustained motion
27 tasks. Transportation research part B: methodological 184, 102969.
- 28 Feng, S., Song, Z., Li, Z., Zhang, Y., Li, L., 2021. Robust platoon control in mixed traffic flow based on tube model predictive control. IEEE
29 Transactions on Intelligent Vehicles 6, 711–722.
- 30 Fine, T.L., 2006. Feedforward neural network methodology. Springer Science & Business Media.
- 31 Gao, B., Cai, K., Qu, T., Hu, Y., Chen, H., 2020. Personalized adaptive cruise control based on online driving style recognition technology and
32 model predictive control. IEEE transactions on vehicular technology 69, 12482–12496.
- 33 Geng, M., Li, J., Xia, Y., Chen, X.M., 2023. A physics-informed transformer model for vehicle trajectory prediction on highways. Transportation
34 research part C: emerging technologies 154, 104272.
- 35 Gindelé, T., Brechtel, S., Dillmann, R., 2010. A probabilistic model for estimating driver behaviors and vehicle trajectories in traffic environments,
36 in: 13th International IEEE Conference on Intelligent Transportation Systems, IEEE. pp. 1625–1631.
- 37 Gu, C., Zhou, T., Wu, C., 2023. Deep koopman traffic modeling for freeway ramp metering. IEEE Transactions on Intelligent Transportation
38 Systems .
- 39 Guo, Q., Ban, X.J., 2023. A multi-scale control framework for urban traffic control with connected and automated vehicles. Transportation research
40 part B: methodological 175, 102787.
- 41 Jarl, S., Aronsson, L., Rahrovani, S., Chehreghani, M.H., 2022. Active learning of driving scenario trajectories. Engineering Applications of
42 Artificial Intelligence 113, 104972.
- 43 Jiang, R., Hu, M.B., Zhang, H., Gao, Z.Y., Jia, B., Wu, Q.S., 2015. On some experimental features of car-following behavior and how to model
44 them. Transportation Research Part B: Methodological 80, 338–354.
- 45 Koopman, B.O., 1931. Hamiltonian systems and transformation in hilbert space. Proceedings of the National Academy of Sciences 17, 315–318.
- 46 Li, G., Chen, Y., Cao, D., Qu, X., Cheng, B., Li, K., 2021. Extraction of descriptive driving patterns from driving data using unsupervised algorithms.
47 Mechanical Systems and Signal Processing 156, 107589.
- 48 Li, K., Wang, J., Zheng, Y., 2022. Cooperative formation of autonomous vehicles in mixed traffic flow: Beyond platooning. IEEE Transactions on
49 Intelligent Transportation Systems 23, 15951–15966.
- 50 Li, S., Wang, J., Yang, K., Xu, Q., Wang, J., Li, K., 2025. Robust nonlinear data-driven predictive control for mixed vehicle platoons via koopman
51 operator and reachability analysis. arXiv preprint arXiv:2502.16466 .
- 52 Li, S., Yanagisawa, D., Nishinari, K., 2024. A jam-absorption driving system for reducing multiple moving jams by estimating moving jam
53 propagation. Transportation Research Part C: Emerging Technologies 158, 104394.
- 54 Lichtlé, N., Vinitsky, E., Nice, M., Seibold, B., Work, D., Bayen, A.M., 2022. Deploying traffic smoothing cruise controllers learned from trajectory
55 data, in: 2022 International Conference on Robotics and Automation (ICRA), IEEE. pp. 2884–2890.
- 56 Lin, L., Li, W., Bi, H., Qin, L., 2021. Vehicle trajectory prediction using lstms with spatial-temporal attention mechanisms. IEEE Intelligent
57 Transportation Systems Magazine 14, 197–208.

- 1 Ling, E., Zheng, L., Ratliff, L.J., Coogan, S., 2020. Koopman operator applications in signalized traffic systems. *IEEE Transactions on Intelligent*
2 *Transportation Systems* 23, 3214–3225.
- 3 Liu, S., Johns, E., Davison, A.J., 2019. End-to-end multi-task learning with attention, in: *Proceedings of the IEEE/CVF conference on computer*
4 *vision and pattern recognition*, pp. 1871–1880.
- 5 Lusch, B., Kutz, J.N., Brunton, S.L., 2018. Deep learning for universal linear embeddings of nonlinear dynamics. *Nature communications* 9, 4950.
- 6 Ma, X., He, X., 2024. Providing real-time en-route suggestions to cavs for congestion mitigation: A two-way deep reinforcement learning approach.
7 *Transportation Research Part B: Methodological* 189, 103014.
- 8 Mo, Z., Shi, R., Di, X., 2021. A physics-informed deep learning paradigm for car-following models. *Transportation research part C: emerging*
9 *technologies* 130, 103240.
- 10 Montanari, F., German, R., Djanatliev, A., 2020. Pattern recognition for driving scenario detection in real driving data, in: *2020 IEEE Intelligent*
11 *Vehicles Symposium (IV)*, IEEE. pp. 590–597.
- 12 Nishi, R., Tomoeda, A., Shimura, K., Nishinari, K., 2013. Theory of jam-absorption driving. *Transportation Research Part B: Methodological* 50,
13 116–129.
- 14 Park, S.H., Kim, B., Kang, C.M., Chung, C.C., Choi, J.W., 2018. Sequence-to-sequence prediction of vehicle trajectory via lstm encoder-decoder
15 architecture, in: *2018 IEEE intelligent vehicles symposium (IV)*, IEEE. pp. 1672–1678.
- 16 Proctor, J.L., Brunton, S.L., Kutz, J.N., 2018. Generalizing koopman theory to allow for inputs and control. *SIAM Journal on Applied Dynamical*
17 *Systems* 17, 909–930.
- 18 Ruan, T., Wang, H., Zhou, L., Zhang, Y., Dong, C., Zuo, Z., 2022. Impacts of information flow topology on traffic dynamics of cav-mv heterogeneous
19 flow. *IEEE Transactions on Intelligent Transportation Systems* 23, 20820–20835.
- 20 Saifuzzaman, M., Zheng, Z., 2014. Incorporating human-factors in car-following models: a review of recent developments and research needs.
21 *Transportation research part C: emerging technologies* 48, 379–403.
- 22 Shen, J., Du, L., 2024. Sequential feasibility and constraint properties of cav platoons under various vehicle dynamics and safety distance constraints.
23 *Transportation research part B: methodological* 185, 102966.
- 24 Shi, H., Zhou, Y., Wu, K., Wang, X., Lin, Y., Ran, B., 2021. Connected automated vehicle cooperative control with a deep reinforcement learning
25 approach in a mixed traffic environment. *Transportation Research Part C: Emerging Technologies* 133, 103421.
- 26 Stern, R.E., Cui, S., Delle Monache, M.L., Bhadani, R., Bunting, M., Churchill, M., Hamilton, N., Pohlmann, H., Wu, F., Piccoli, B., et al.,
27 2018. Dissipation of stop-and-go waves via control of autonomous vehicles: Field experiments. *Transportation Research Part C: Emerging*
28 *Technologies* 89, 205–221.
- 29 Talebian, A., Mishra, S., 2018. Predicting the adoption of connected autonomous vehicles: A new approach based on the theory of diffusion of
30 innovations. *Transportation Research Part C: Emerging Technologies* 95, 363–380.
- 31 Tian, K., Shi, H., Zhou, Y., Li, S., 2024. Physically analyzable ai-based nonlinear platoon dynamics modeling during traffic oscillation: A koopman
32 approach. *arXiv preprint arXiv:2406.14696*.
- 33 Treiber, M., Hennecke, A., Helbing, D., 2000. Congested traffic states in empirical observations and microscopic simulations. *Physical review E*
34 62, 1805.
- 35 Vaswani, A., Shazeer, N., Parmar, N., Uszkoreit, J., Jones, L., Gomez, A.N., Kaiser, Ł., Polosukhin, I., 2017. Attention is all you need. *Advances*
36 *in neural information processing systems* 30.
- 37 Wang, J., Lian, Y., Jiang, Y., Xu, Q., Li, K., Jones, C.N., 2023a. Distributed data-driven predictive control for cooperatively smoothing mixed traffic
38 flow. *Transportation Research Part C: Emerging Technologies* 155, 104274.
- 39 Wang, J., Lu, L., Peeta, S., 2022. Real-time deployable and robust cooperative control strategy for a platoon of connected and autonomous vehicles
40 by factoring uncertain vehicle dynamics. *Transportation Research Part B: Methodological* 163, 88–118.
- 41 Wang, J., Zheng, Y., Chen, C., Xu, Q., Li, K., 2021. Leading cruise control in mixed traffic flow: System modeling, controllability, and string
42 stability. *IEEE Transactions on Intelligent Transportation Systems* 23, 12861–12876.
- 43 Wang, J., Zheng, Y., Li, K., Xu, Q., 2023b. Deep-lcc: Data-enabled predictive leading cruise control in mixed traffic flow. *IEEE Transactions on*
44 *Control Systems Technology*.
- 45 Wang, J., Zheng, Y., Xu, Q., Wang, J., Li, K., 2020. Controllability analysis and optimal control of mixed traffic flow with human-driven and
46 autonomous vehicles. *IEEE Transactions on Intelligent Transportation Systems* 22, 7445–7459.
- 47 Wang, J., Zhou, A., Liu, Z., Peeta, S., 2024a. Robust cooperative control strategy for a platoon of connected and autonomous vehicles against sensor
48 errors and control errors simultaneously in a real-world driving environment. *Transportation research part B: methodological* 184, 102946.
- 49 Wang, S., Wang, Z., Jiang, R., Zhu, F., Yan, R., Shang, Y., 2024b. A multi-agent reinforcement learning-based longitudinal and lateral control of
50 cavs to improve traffic efficiency in a mandatory lane change scenario. *Transportation Research Part C: Emerging Technologies* 158, 104445.
- 51 Wang, Y., Jiang, Y., Wu, Y., Yao, Z., 2024c. Mitigating traffic oscillation through control of connected automated vehicles: A cellular automata
52 simulation. *Expert Systems with Applications* 235, 121275.
- 53 Wang, Z., Bian, Y., Shladover, S.E., Wu, G., Li, S.E., Barth, M.J., 2019. A survey on cooperative longitudinal motion control of multiple connected
54 and automated vehicles. *IEEE Intelligent Transportation Systems Magazine* 12, 4–24.
- 55 Williams, M.O., Kevrekidis, I.G., Rowley, C.W., 2015. A data-driven approximation of the koopman operator: Extending dynamic mode decom-
56 position. *Journal of Nonlinear Science* 25, 1307–1346.
- 57 Xiao, Y., Zhang, X., Xu, X., Liu, X., Liu, J., 2022. Deep neural networks with koopman operators for modeling and control of autonomous vehicles.
58 *IEEE Transactions on Intelligent Vehicles* 8, 135–146.
- 59 Xing, Y., Lv, C., Cao, D., 2019. Personalized vehicle trajectory prediction based on joint time-series modeling for connected vehicles. *IEEE*
60 *Transactions on Vehicular Technology* 69, 1341–1352.
- 61 Yan, R., Wang, S., 2022. Integrating prediction with optimization: Models and applications in transportation management.
- 62 Yue, X., Shi, H., Zhou, Y., Li, Z., 2024. Hybrid car following control for cavs: Integrating linear feedback and deep reinforcement learning to
63 stabilize mixed traffic. *Transportation Research Part C: Emerging Technologies* 167, 104773.

- 1 Zhan, J., Ma, Z., Zhang, L., 2022. Data-driven modeling and distributed predictive control of mixed vehicle platoons. *IEEE Transactions on*
2 *Intelligent Vehicles* 8, 572–582.
- 3 Zhang, X., Sun, J., Qi, X., Sun, J., 2019. Simultaneous modeling of car-following and lane-changing behaviors using deep learning. *Transportation*
4 *research part C: emerging technologies* 104, 287–304.
- 5 Zhang, Y., Chen, X., Wang, J., Zheng, Z., Wu, K., 2022. A generative car-following model conditioned on driving styles. *Transportation research*
6 *part C: emerging technologies* 145, 103926.
- 7 Zhao, C., Yu, H., 2024. Robust safety for mixed-autonomy traffic with delays and disturbances. *IEEE Transactions on Intelligent Transportation*
8 *Systems* .
- 9 Zheng, Y., Wang, J., Li, K., 2020. Smoothing traffic flow via control of autonomous vehicles. *IEEE Internet of Things Journal* 7, 3882–3896.
- 10 Zhou, M., Qu, X., Jin, S., 2016. On the impact of cooperative autonomous vehicles in improving freeway merging: a modified intelligent driver
11 *model-based approach*. *IEEE Transactions on Intelligent Transportation Systems* 18, 1422–1428.
- 12 Zou, Y., Zhu, T., Xie, Y., Zhang, Y., Zhang, Y., 2022. Multivariate analysis of car-following behavior data using a coupled hidden markov model.
13 *Transportation research part C: emerging technologies* 144, 103914.